Atmospheric
Chemistry
and Physics

Shipborne measurements of total OH reactivity around the Arabian Peninsula and its role in ozone chemistry

Eva Y. Pfannerstill[1], **Nijing Wang**[1], **Achim Edtbauer**[1], **Efstratios Bourtsoukidis**[1], **John N. Crowley**[1], **Dirk Dienhart**[1], **Philipp G. Eger**[1], **Lisa Ernle**[1], **Horst Fischer**[1], **Bettina Hottmann**[1], **Jean-Daniel Paris**[2], **Christof Stönner**[1], **Ivan Tadic**[1], **David Walter**[1], **Jos Lelieveld**[1,3], and **Jonathan Williams**[1,3]

[1]Atmospheric Chemistry and Multiphase Chemistry Departments, Max Planck Institute for Chemistry,
55128 Mainz, Germany
[2]Laboratoire des Sciences du Climat et de l'Environnement, LSCE/IPSL, CEA-CNRS-UVSQ,
Université Paris-Saclay, Gif-sur-Yvette, France
[3]Energy, Environment and Water Research Center, The Cyprus Institute, Nicosia, Cyprus

Correspondence: Eva Y. Pfannerstill (eva.pfannerstill@mpic.de)

Abstract. The Arabian Peninsula is characterized by high and increasing levels of photochemical air pollution. Strong solar irradiation, high temperatures and large anthropogenic emissions of reactive trace gases result in intense photochemical activity, especially during the summer months. However, air chemistry measurements in the region are scarce. In order to assess regional pollution sources and oxidation rates, the first ship-based direct measurements of total OH reactivity were performed in summer 2017 from a vessel traveling around the peninsula during the AQABA (Air Quality and Climate Change in the Arabian Basin) campaign. Total OH reactivity is the total loss frequency of OH radicals due to all reactive compounds present in air and defines the local lifetime of OH, the most important oxidant in the troposphere. During the AQABA campaign, the total OH reactivity ranged from below the detection limit ($5.4\,\mathrm{s}^{-1}$) over the northwestern Indian Ocean (Arabian Sea) to a maximum of $32.8 \pm 9.6\,\mathrm{s}^{-1}$ over the Arabian Gulf (also known as Persian Gulf) when air originated from large petroleum extraction/processing facilities in Iraq and Kuwait. In the polluted marine regions, OH reactivity was broadly comparable to highly populated urban centers in intensity and composition. The permanent influence of heavy maritime traffic over the seaways of the Red Sea, Gulf of Aden and Gulf of Oman resulted in median OH sinks of 7.9–$8.5\,\mathrm{s}^{-1}$. Due to the rapid oxidation of direct volatile organic compound (VOC) emissions, oxygenated volatile organic compounds (OVOCs) were observed to be the main contributor to OH reactivity around the Arabian Peninsula (9 %–35 % by region). Over the Arabian Gulf, alkanes and alkenes from the petroleum extraction and processing industry were an important OH sink with $\sim 9\,\%$ of total OH reactivity each, whereas NO_x and aromatic hydrocarbons ($\sim 10\,\%$ each) played a larger role in the Suez Canal, which is influenced more by ship traffic and urban emissions. We investigated the number and identity of chemical species necessary to explain the total OH sink. Taking into account ~ 100 individually measured chemical species, the observed total OH reactivity can typically be accounted for within the measurement uncertainty (50 %), with 10 dominant trace gases accounting for 20 %–39 % of regional total OH reactivity. The chemical regimes causing the intense ozone pollution around the Arabian Peninsula were investigated using total OH reactivity measurements. Ozone vs. OH reactivity relationships were found to be a useful tool for differentiating between ozone titration in fresh emissions and photochemically aged air masses. Our results show that the ratio of NO_x- and VOC-attributed OH reactivity was favorable for ozone formation almost all around the Arabian Peninsula, which is due to NO_x and VOCs from ship exhausts and, often, oil/gas production. Therewith, total OH reactivity measurements help to elucidate the chemical processes underlying the extreme tropospheric ozone concentrations observed in summer over the Arabian Basin.

1 Introduction

The Arabian Peninsula is a hotspot of global change. It is already subject to extremes of heat and drought, which are predicted to intensify (Zhang et al., 2005; Wasimi, 2010; Chenoweth et al., 2011; Tanarhte et al., 2012; Lelieveld et al., 2012, 2016; Terink et al., 2013; Donat et al., 2014; Cook et al., 2016), and to photochemical air pollution (Lelieveld et al., 2009; Smoydzin et al., 2012; Abdelkader et al., 2015; Farahat, 2016). The Middle East accommodates densely populated urban centers with a total of 350 million people, and is a hub of fossil fuel extraction and processing with more than half of the world's known oil and gas reserves (Khatib, 2014). Moreover, the waters surrounding the Arabian Peninsula are key routes of global trade and bottlenecks for marine traffic, another source of air pollution (Endresen, 2003; Eyring, 2005; Boersma et al., 2015; Mertens et al., 2018) that is expected to increase in the future (Eyring et al., 2007).

Photochemistry in the region is thought to be particularly active due to a combination of factors: large anthropogenic emissions of reactive hydrocarbons and NO_x ($= NO + NO_2$) from the petroleum industry; shipping and energy-intensive urban areas, with high levels of solar irradiation and hence photolysis rates; and high temperature, which disfavors NO_x reservoirs such as PAN and N_2O_5. The main regional photochemical oxidation process is initiated by ozone photolysis to $O(^1D)$, which reacts with water vapor to form hydroxyl radicals (OH). The OH radicals react with volatile organic compounds (VOCs) to yield peroxy radicals that can convert NO to NO_2, leading to ozone formation (Haagen-Smit, 1952; Sillman, 1999; Ren et al., 2013). The abundance of precursors and intense photochemistry make conditions in the Arabian Basin very favorable for photochemical ozone production, leading to extremely high ozone mixing ratios up to 200 ppb (Lelieveld et al., 2009; Smoydzin et al., 2012; Krotkov et al., 2016). Ozone formation was reported to be enhanced even 300 km downwind of a hydrocarbon processing facility at the coast of the Arabian Gulf (Moradzadeh et al., 2019). In addition, VOC oxidation by OH and ozone can generate secondary organic aerosol (Grosjean and Seinfeld, 1989; Kroll and Seinfeld, 2008) with implications for human health (Lelieveld et al., 2015) and regional radiative budgets (Ezhova et al., 2018).

Despite being an air pollution hotspot, very few observational atmospheric data exist from the Arabian Basin, and studies of VOCs in the region are scarce and mostly urban (Doskey et al., 1999; Matysik et al., 2010; Salameh et al., 2014, 2016; Simpson et al., 2014; Khalil et al., 2016; Barletta et al., 2017). In order to chemically map the region, a comprehensive suite of atmospheric measurements was performed from a ship sailing around the Arabian Peninsula in summer 2017 during the AQABA (Air Quality and Climate Change in the Arabian Basin) cruise.

The number of known VOCs in air has been estimated to be between 10^4 and 10^5 species (Goldstein and Galbally,

2007), and it is assumed that many more remain unknown. Accounting for all of these chemical compounds individually with quantitative measurements is currently unfeasible. Instead, the combined load of OH reactive species (mainly VOCs and CO) in ambient air, termed the total OH reactivity, can be measured directly. Total OH reactivity denotes the total sink, or loss frequency, of the OH radical. When compared to the OH reactivity calculated from all individually measured compounds (termed the speciated OH reactivity), total OH reactivity can be used to infer the occurrence of VOCs that were not measured (termed the unattributed or "missing" OH reactivity). Moreover, total OH reactivity is necessary for a quantitative understanding of ozone production and can help estimate its sensitivity to VOCs and NO_x (Kirchner et al., 2001; Sinha et al., 2010; Pusede et al., 2014; Yang et al., 2017). The OH sink also affects the atmospheric residence time of methane and therewith its global budget, which still poses a challenge in models (Zhao et al., 2019).

With VOC and NO_x emissions from ship exhausts (Boersma et al., 2015; Endresen, 2003; Huang et al., 2018) and VOCs from oil and gas operations (Buzcu and Fraser, 2006; Gilman et al., 2009, 2013; Schade and Roest, 2016; Milazzo et al., 2017), the air around the Arabian Peninsula is expected to contain significant levels of pollution. In Saudi Arabian cities, OH reactivity has been reported to range from 14 to $42\,s^{-1}$ (from the sum of individual measurements), dominated by alkenes (Barletta et al., 2017). Downwind of oil and gas production in Colorado, OH reactivity of VOCs was dominated by alkanes (60 %), followed by OVOCs (27 %) and alkenes (8 %; Gilman et al., 2013). The largest OH sink among the VOCs in the exhaust plume of a ship operating at full speed is alkenes (42 %), followed by aromatics (40 %), OVOCs (12 %) and alkanes (5 %; estimated using emission factors from Huang et al., 2018).

Unattributed OH reactivity in locations dominated by anthropogenic VOCs has been measured to be as low as zero in Lille, France (Hansen et al., 2015), or New York, US (Ren et al., 2006), to 10 %–54 % in Paris, France (Dolgorouky et al., 2012), and 10 %–80 % in Tokyo, Japan (Yoshino et al., 2006). However, comparing unattributed OH reactivity between different studies is difficult because it depends on the air mass and coverage of inorganic trace gases and VOCs measured in each campaign. In this work, we apply an approach that aims to use comprehensive trace gas information gathered by various instruments, even compounds with unidentified chemical structure measured by PTR-ToF-MS, for calculation of speciated OH reactivity. Therewith, we identify the trace gases representing the major OH sinks and try to obtain closure on apportioning OH reactivity.

This study provides an overview of total OH reactivity around the Arabian Peninsula and investigates its sources in the different environments along the route of the campaign. Total OH reactivity is applied for assessing the regional oxidation chemistry and the underlying reasons for the extreme ozone concentrations observed in summer over

the Arabian Basin. By combining OH reactivity and ozone measurements, we aim to investigate ozone production processes and to identify differentiated chemical regimes. We demonstrate the utility of in situ OH reactivity measurements to characterize the role of anthropogenic emissions in modifying the chemical composition of the air.

2 Materials and methods

2.1 AQABA campaign

The Air Quality and Climate Change in the Arabian Basin (AQABA) measurements took place on board the vessel *Kommandor Iona* from 25 June till 3 September 2017. The first leg began in La-Seyne-sur-Mer (near Toulon, France) and continued via the Mediterranean, the Suez Canal, the Red Sea, the Indian Ocean, the Gulf of Oman and the Arabian Gulf to Kuwait. On the second leg, the vessel returned via the same route (Fig. 1a, b). The ship was equipped with a weather station and four laboratory containers with instrumentation for in situ and offline monitoring of a large suite of (trace) gases, particles and radicals.

2.2 Sampling

Air sampling was performed from a high-flow ($10 \, m^3 \, min^{-1}$) cylindrical stainless steel inlet (sampling height: 5.5 m above deck, diameter: 0.2 m), situated between the containers on the front deck of the ship. This position ensured that inlets were ahead of any contamination sources from the vessel itself when pointed into the wind. Air was drawn from the center of the high-flow inlet and subsampled at a rate of approximately 5 slpm (standard liters per minute, first leg) and 3 slpm (second leg) into an air conditioned laboratory container using a FEP (fluorinated ethylene propylene) inlet tube ($1/2'' = 1.27 \, cm$ o.d., length ca. 10 m), heated to 50–60 °C. A PTFE (polytetrafluoroethylene) filter, changed weekly (and additionally after intense particle contamination events such as dust storms), prevented contamination of the subsampling line by particles or sea spray. This inlet system was used for monitoring both VOCs and total OH reactivity simultaneously. We assume that the length of the inlet prevented some of the larger, extremely low-volatility VOCs from reaching the instruments (see Sect. 3.3). The combined inlet residence time in FEP tubing and reactor for the OH reactivity instrument was determined as ≈ 15 s during the first leg and ≈ 25 s during the second leg by spiking with acetone.

2.3 OH reactivity and trace gas measurements

Total OH reactivity was measured using the comparative reactivity method (CRM; Sinha et al., 2008), which proved to be robust enough to run nearly continuously for 10 weeks on a ship, often in rough conditions due to high waves. The method has been applied in many regions of the world (Yang

et al., 2016) and has recently been compared to other methods (Fuchs et al., 2017). The CRM is based on a competitive reaction between reactive compounds from ambient air and a reagent, pyrrole (Westfalen AG, Münster, Germany), inside a glass reactor. OH radicals are produced in the reactor by flushing humidified nitrogen (6.0 grade, Westfalen AG, Münster, Germany) over a Hg–Ar UV lamp (LOT Quantum Design, Darmstadt, Germany). CRM uses three different modes: C1 (pyrrole + OH scavenger + UV light, at ≈ ambient humidity), C2 (OH + pyrrole, ambient humidity) and C3 (ambient air + pyrrole + OH). For more details of the method see Sinha et al. (2008) and Michoud et al. (2015). The system was operated at a pyrrole / OH ratio of 1.9 ± 0.1 (average ± standard deviation). Because this ratio deviates from pseudo-first-order conditions, as is typical for CRM, a correction needed to be applied (see Sect. 2.4). Sampling air was continuously drawn into the system, and the instrument was switched between C3 (measured for 22–24 min) and C2 (measured for 6–8 min) modes. The longer C2 measurements were used when ambient humidity was unstable. C1 was determined every 5–7 d (average ± standard deviation over the whole campaign: 60.71 ± 1.18 ppb of pyrrole). Changes in pyrrole mixing ratio were monitored by a proton-transfer-reaction quadrupole mass spectrometer (PTR-QMS, Ionicon Analytik, Innsbruck, Austria; Lindinger and Jordan, 1998) at $m/z = 68$ (dwell time: 5 s). The PTR-QMS was calibrated every week. It was operated at 60 °C drift temperature, 2.2 mbar drift pressure and 600 V drift voltage (E/N = 137 Td). In parallel, a PTR time-of-flight (ToF) MS was deployed to monitor VOCs and OVOCs (m/z up to 280), and a gas chromatograph with a flame ionization detector (GC–FID) was used to monitor non-methane hydrocarbons (NMHCs; 20 compounds). Average detection limits for the different NMHCs ranged from 1 to 25 ppt. The NMHC and methane measurements are described in detail elsewhere (Bourtsoukidis et al., 2019). The PTR-ToF-MS was deployed at 60 °C drift temperature, 2.2 mbar drift pressure and 600 V drift voltage (E/N = 137 Td). 1,3,5-Trichlorobenzene was fed continuously into the sample stream for mass scale calibration. The time resolution of the measurement was 1 min and background measurements were performed every 3 h for 10 min. The PTR-ToF-MS was calibrated with a multicomponent pressurized gas VOC standard (Apel-Riemer Environmental Inc., Colorado, USA). Mass resolution (full width at half maximum) at 96 amu ranged between ∼ 3500 and ∼ 4500. Average detection limits for the compounds measured by PTR-ToF-MS ranged from 1 to 107 ppt. A full list of the trace gases measured by GC–FID and PTR-ToF-MS can be found in Table S1 in the Supplement.

Formaldehyde (HCHO) and inorganic trace gases (NO, NO_2, O_3, SO_2) were measured sampling from the same chimney (the instruments used are specified in Table S1). Based on SO_2, NO_x and ethene measurements, a filter was applied to exclude sampling periods that were influenced by the vessel's own exhaust.
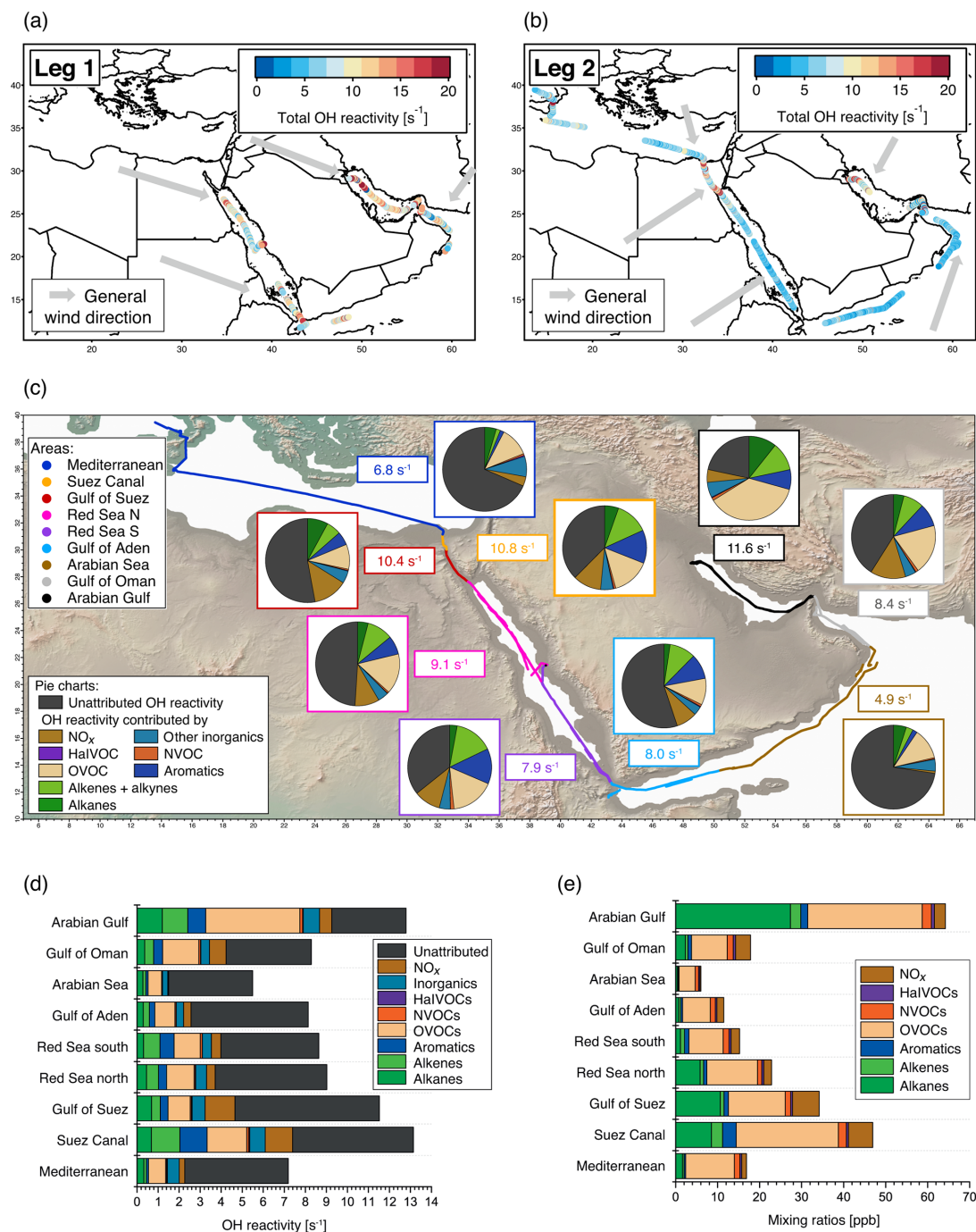
Figure 1. Overview of total OH reactivity around the Arabian Peninsula during the AQABA campaign. OH reactivity during **(a)** leg 1 (5–31 July 2017) and **(b)** leg 2 (3–31 August 2017). The maximum in the color scales is set to $20\,\text{s}^{-1}$ for better visibility of differences, although there are a few data points above this value. Arrows depict general wind directions for the respective regions. **(c)** Total OH reactivity medians by region, and pie charts showing the contribution of compound classes for data points where speciated OH reactivity ≥ LOD (exception: pie charts of Mediterranean and Arabian seas show the average of all data points, due to the low number of points above LOD). **(d)** Average OH reactivity and speciation by region for all data points, including those where speciated OH reactivity was below the LOD. Error bars show the total uncertainty of the measurement. **(e)** Average mixing ratio of VOCs / trace gases in parts per billion by compound class and region (except for the class of inorganic compounds other than NO_x). The individual compounds included in each class are listed in Table S1. Port calls and bunkering are excluded from all averages.

2.4 Total OH reactivity data analysis

CRM data analysis was conducted following the general procedures described in Keßel (2016) and Pfannerstill et al. (2018).

Humidity in C2 (background) measurements can differ from that of C3 (ambient) measurements because C2 was measured only twice per hour. As the amount of OH radicals generated in the CRM reactor depends on humidity, C2 data were corrected for these C2–C3 humidity differences by applying an empirical relationship of the pyrrole signal vs. the PTR-MS water cluster signal as described in Michoud et al. (2015). The C2 correction applied to match C3 humidity decreased pyrrole levels by on average 0.05 ± 0.04 ppb, corresponding to an OH reactivity of $\approx 0.3 \, \text{s}^{-1}$. NO, NO_2 and ozone cause interferences in CRM due to OH recycling induced by HO_2, which is formed in the reactor simultaneously with OH (Sinha et al., 2008; Michoud et al., 2015; Fuchs et al., 2017). Ozone, NO and NO_2 interferences were quantified in the laboratory (details of the experiments can be found in Sect. S1 in the Supplement). NO_2 loss and conversion to NO in the mass flow controller during tests was monitored by an NO–NO_2 analyzer (two-channel-chemiluminescence detector). The combined NO, NO_2 and ozone corrections amounted to a median of $\sim 24\%$ of total OH reactivity or an average of 0.36 ± 0.19 ppb of pyrrole over the whole campaign, which equals $\approx 1.9 \, \text{s}^{-1}$, with a maximum absolute correction of 1.39 ppb ($7.4 \, \text{s}^{-1}/27\%$ of total OH reactivity) under the influence of closely located ship emissions (high NO_x). A frequency distribution of the corrected fraction of total OH reactivity is displayed in Fig. S1 in the Supplement.

The calculation of total OH reactivity with the CRM equation (see Sinha et al., 2008) assumes pseudo-first-order conditions inside the reactor, which can, however, not be met while preserving a reasonable sensitivity (C3–C2 difference). The correction for deviation from pseudo-first-order conditions inside the reactor was derived from empirical test gas measurements adapted from the approach in Michoud et al. (2015). The deviation from pseudo-first-order depends on the pyrrole / OH ratio and on the reaction rate constant of the measured trace gas towards OH. Trace gases with fast reaction rates (comparable to that of pyrrole) require the largest correction because their concentration inside the reactor decreases at a similar rate as that of pyrrole, leading to an underestimation of their reactivity. Such gases, namely alkenes, were sometimes present during AQABA (e.g., a C_5H_8-alkene which was not isoprene). This is why we did not use an average correction factor for all gas mixes as in Michoud et al. (2015), but applied a correction where the composition of the air mass is taken into account. Test gases used were toluene (for aromatic correction), isoprene and propene (for alkene correction), and propane and cyclohexane (correction for other species). These test gases are representative of the relevant trace gases and ranges of reaction rate coefficients observed during AQABA. In test experiments, these trace gases were added to the CRM system in known amounts, i.e., known total OH reactivities, at pyrrole / OH ratios representative for the campaign. The correction factors resulting from comparing the observed reactivity with the expected reactivity were weighted according to the measured composition of the ambient air at the moment of observation:

$$F = a \, X_{\text{aromatic}} + b \, X_{\text{alkenes}} + c \, (1 - X_{\text{arom}} - X_{\text{alkenes}}), \quad (1)$$

where F is the total correction factor and the weighted compound-class-specific correction factors are $a = 1.22$, $b = 2.89$ and $c = 1.44$. X is the speciated OH reactivity fraction (s^{-1} s of the respective class of compounds (aromatics, alkenes). This correction increased OH reactivity by a factor of 1.4 to 2.5 (average $\pm$ standard deviation: $F = 1.5 \pm 0.1$, median = 1.5).

The dilution of ambient air with humidified nitrogen was accounted for with a dilution factor of 1.34.

The 5 min detection limit (LOD) was $5.4 \, \text{s}^{-1}$, derived from the 2σ standard deviation of clean air measurements in the Arabian Sea. Total uncertainty (1σ) of the measurements was $\sim 50\%$ (median and average), with a precision of 10%–76% over 5 min depending on the quantity of reactivity.

2.5 Calculated OH reactivity from individually measured compounds (speciated OH reactivity)

The speciated OH reactivity is the sum of the OH reactivities attributed to individual (measured) trace gases:

$$R = \Sigma k_{\text{M+OH}}[\text{M}]). \quad (2)$$

Contributions of trace gases (M, where [M] is their respective concentration in molecules per cubic centimeter) to OH reactivity (R in reciprocal seconds) are calculated using the reaction rate constants ($k_{\text{M+OH}}$ in $\text{cm}^3 \, \text{molecule}^{-1} \, \text{s}^{-1}$) of the respective trace gases (M) with the OH radical. The difference between measured total OH reactivity and the sum of individual trace gas contributions to OH reactivity is termed unattributed or missing OH reactivity. The trace gases taken into account here for calculating speciated OH reactivity and their reaction rate constants used are listed in Table S1. Out of a total of 120 chemical species that were considered for the calculation of speciated reactivity, 42 chemical species (specified in Table S1), including many of the known important contributors to OH reactivity, were calibrated with gas standards and therefore have low uncertainties in their concentrations as well as in their reaction rate coefficients (5%–15%). A further 78 exact masses (specified in Table S1) monitored by PTR–ToF–MS were attributed to molecular formulae, and their concentrations derived using a theoretical approach (Lindinger and Jordan, 1998), which has an uncertainty of ca. 50%. In cases where several trace gases could be responsible for the measured mass, an average of the known reaction rate coefficients with OH was used for calculating the speciated OH reactivity. In the few cases where rate coefficients were unknown in literature, the rate coefficient of

a trace gas with comparable functional groups was applied (see Table S1). The uncertainty of the reaction rate coefficients k_{M+OH} is estimated to be 100 % due to the occasional large differences in rate coefficients between possible structures. The uncertainty of the resulting speciated (i.e., calculated) OH reactivity depends on the fraction of gas-standard calibrated compounds in the ambient air at any given point of time and varies between 10 % and 92 %, with an average and median of 45 % over the whole campaign. In accordance with the time resolution of the GC–FID, which monitored compounds with a significant share of OH reactivity, speciated OH reactivity was calculated in 50 min time resolution.

2.6   Air mass back trajectories

To investigate the origin of air masses encountered, back trajectories were derived using the Hybrid Single-Particle Lagrangian Integrated Trajectory model (HYSPLIT, version 4, 2014). This model is a hybrid between a Lagrangian and an Eulerian model for tracing small imaginary air parcels forward or back in time (Draxler and Hess, 1998). Back trajectories were calculated based on a start height of 200 m above sea level, going 216 h back in time on an hourly grid beginning at the ship position.

3   Results and discussion

3.1   Overview of total OH reactivity around the Arabian Peninsula

The air masses encountered during the AQABA campaign were delineated according to the geographical region (Fig. 1a, b). A notable difference between leg 1 and leg 2 was the general wind direction over the Arabian Gulf, which changed from northwest (from Iraq–Kuwait) to northeast (from Iran). The range of observed total OH reactivities over the whole campaign was from below the detection limit over the Arabian Sea (northwest Indian Ocean) up to $303.6 \pm 83.9 \, \text{s}^{-1}$ during fueling/bunkering of the ship at the port of Fujairah (United Arab Emirates), due to fresh fuel emissions. The largest fraction of attributed OH reactivity was provided by OVOCs in almost all AQABA regions (9 %–35 %), which is comparable to previous studies in the oil-impacted region of Houston, where between 11 % and 24 % of the OH sink was due to OVOCs (Mao et al., 2010). There were notable regional differences in both the total OH reactivity and the contributing trace gases, which will be discussed hereafter. An overview is displayed in Table 1, which divides the reactivity into different chemical families. A list of chemical species attributed to each chemical family is available in Table S1.

The measured sulfur-containing VOCs (SVOCs) and halogenated VOCs (HalVOCs) played virtually no role for OH reactivity in any of the AQABA regions (Table 1). The OH reactivity of the monitored NVOCs (nitrogen-containing

VOCs) was also very minor with not more than 1 % of total OH reactivity over the whole campaign.

3.1.1   Strongly polluted regions: Arabian Gulf, Gulf of Suez and Suez Canal

Compounds with short lifetimes are generally more relevant for total OH reactivity than long-lived species (see also Sect. 3.3). Since emissions from oil and gas production and cities contain high mixing ratios of reactive alkenes, the Arabian Gulf, the Gulf of Suez and the Suez Canal, where such sources abound, showed the highest average OH reactivities (Fig. 1c, d). In these regions, obvious nearby emission sources were cities, industrial complexes, and especially oil/gas production/processing (Fig. 2). The large alkane mixing ratios associated with oil and gas production (Fig. 1e; Bourtsoukidis et al., 2019) were not reflected in an equally large share of total OH reactivity due to the slow reaction rate coefficient of alkanes with the OH radical (Fig. 1d). The average total OH reactivity (± standard deviation) was $12.9 \pm 6.2 \, \text{s}^{-1}$ (median: $11.2 \, \text{s}^{-1}$) over the Arabian Gulf, $13.2 \pm 6.9 \, \text{s}^{-1}$ (median: $10.8 \, \text{s}^{-1}$) over the Suez Canal and $11.6 \pm 4.2 \, \text{s}^{-1}$ (median: $10.4 \, \text{s}^{-1}$) over the Gulf of Suez. There were short periods with higher total OH reactivities (± total uncertainties) up to $32.8 \pm 9.6 \, \text{s}^{-1}$ over the Arabian Gulf and $26.6 \pm 8.2 \, \text{s}^{-1}$ over the Suez Canal (see Sect. 3.2). These ranges are comparable to OH reactivities reported from some urban areas, e.g., Beijing, China (Williams et al., 2016), Houston, Texas (Mao et al., 2010), and New York City (Ren et al., 2006), and to OH reactivities calculated from ship-based VOC observations in Houston–Galveston Bay impacted by fossil fuel production (Gilman et al., 2009). The AQABA observations are, however, more than 3 times as high as VOC-attributed OH reactivity calculated from observations downwind of gas and oil production in south Texas (Schade and Roest, 2016) and twice as high as at the Boulder Atmospheric Observatory when impacted by gas wells (Swarthout et al., 2013).

The largest percentage of attributed OH reactivity over the Arabian Gulf was provided by OVOCs (35 % of total, in contrast to 14 % observed over Houston–Galveston Bay (Gilman et al., 2009). This was surprising, as the Arabian Gulf region was expected to be similarly dominated by direct hydrocarbon emissions from the fossil fuel industry as the Houston–Galveston Bay. Although the alkanes and OVOCs had broadly equivalent mixing ratios over the Arabian Gulf (Fig. 1e), the former have generally lower OH reactivity. Conditions in the Arabian Gulf region during summer favor rapid photooxidation of hydrocarbon emissions to OVOCs, due to high temperatures (on average 34.5 °C), high humidity (up to 92 % RH) and strong irradiation. It should also be noted that as the ship passed through the Arabian Gulf, it was only exposed to primary emissions for relatively short periods of time, when located directly downwind of the sources. The more oxidized regional background air was sampled for

Table 1. Overview of measured and speciated OH reactivity by region. "≥ LOD" signifies the use of exclusively those data points where speciated OH reactivity is equal to or above the LOD. Percentages of contribution to total OH reactivity by group were calculated from all data points in 50 min time resolution. The chemical species attributed to each group are listed in Table S1. For an explanation of unattributed or speciated OH reactivity and "theoretical approach" species, refer to Sect. 2.5. The 10 most important species are the species with the largest average OH reactivity over the respective region. The ratios of C_3 or C_5 carbonyls vs. their precursors or toluene vs. benzene are indicators for air mass age. * Note that the detection limit was $5.4\,\mathrm{s}^{-1}$. (Medit. is Mediterranean.)

	Medit. Sea	Suez Canal	Gulf of Suez	Red Sea north	Red Sea south	Gulf of Aden	Arabian Sea	Gulf of Oman	Arabian Gulf
Aromatic hydrocarbons	1 %	10 %	3 %	4 %	8 %	3 %	2 %	5 %	7 %
Alkanes	4 %	5 %	6 %	5 %	4 %	4 %	5 %	4 %	9 %
Alkenes	2 %	10 %	4 %	6 %	9 %	4 %	3 %	5 %	9 %
OVOCs	11 %	14 %	9 %	14 %	14 %	12 %	12 %	21 %	35 %
NVOCs	1 %	1 %	0 %	1 %	1 %	1 %	1 %	1 %	1 %
SVOCs	0 %	0 %	0 %	0 %	0 %	0 %	1 %	1 %	0 %
Halogenated VOCs	0 %	0 %	0 %	0 %	0 %	0 %	0 %	0 %	0 %
Inorganics	8 %	6 %	5 %	6 %	5 %	4 %	4 %	5 %	6 %
NO_x	4 %	10 %	12 %	5 %	5 %	4 %	1 %	9 %	5 %
Unattributed OH reactivity fraction (all data points) $\pm 1\sigma$ total uncertainty	68 ± 52 %	44 ± 43 %	59 ± 44 %	59 ± 50 %	54 ± 54 %	68 ± 51 %	72 ± 57 %	49 ± 55 %	27 ± 55 %
Unattributed OH reactivity fraction ≥ LOD $\pm 1\sigma$ total uncertainty	none	37 ± 35 %	53 ± 34 %	49 ± 39 %	35 ± 55 %	55 ± 38 %	none	41 ± 52 %	22 ± 56 %
Fraction of species with concentrations derived from theoretical approach	28 %	28 %	22 %	38 %	51 %	46 %	42 %	46 %	46 %
Speciated (calculated) OH reactivity (s^{-1}), averages ± standard deviation	2.3 ± 1.2	7.4 ± 5.8	4.7 ± 2.2	3.7 ± 1.7	4.0 ± 2.1	2.6 ± 1.1	1.5 ± 0.2	4.3 ± 1.2	9.3 ± 5.6
Speciated (calculated) OH reactivity (s^{-1}), medians, 25th–75th percentiles	2.0 1.9–2.2	5.4 2.7–13.4	4.3 3.0–5.9	3.3 2.5–4.5	3.7 2.2–5.5	2.4 2.0–2.9	1.5 1.4–1.7	4.0 3.2–5.2	7.6 5.2–11.9
Measured OH reactivity (s^{-1}), averages ± standard deviation	7.2 ± 2.9	13.2 ± 6.9	11.6 ± 4.2	9.1 ± 3.3	8.7 ± 4.2	8.2 ± 3.1	5.6* ± 2.0	8.3 ± 3.6	12.9 ± 6.2
Measured OH reactivity (s^{-1}), medians, 25th–75th percentile	6.8 5.8–7.8	10.8 7.4–18.8	10.4 8.2–15.0	8.5 7.0–10.5	7.9 5.7–10.9	8.0 5.9–10.1	4.9* 4.1–6.5	8.4 5.9–10.5	11.2 8.9–15.2
OH reactivity of 10 most important species (s^{-1})	1.7	3.8	3.1	2.1	2.2	1.7	1.1	3.3	4.9
Fraction of total OH reactivity contributed by 10 most important species	24 %	29 %	27 %	23 %	25 %	21 %	20 %	39 %	38 %
C_3 carbonyls/propane ($\mathrm{ppb\,ppb}^{-1}$), medians	8.6	3.4	2.6	1.9	9.4	6.8	none	2.4	0.9
C_5 carbonyls/pentanes ($\mathrm{ppb\,ppb}^{-1}$), medians	3.0	1.7	1.1	1.3	1.9	2.4	3.8	1.2	2.8
Toluene/benzene ($\mathrm{ppb\,ppb}^{-1}$), medians	0.24	0.88	0.80	0.39	0.78	0.33	0.18	0.79	0.47
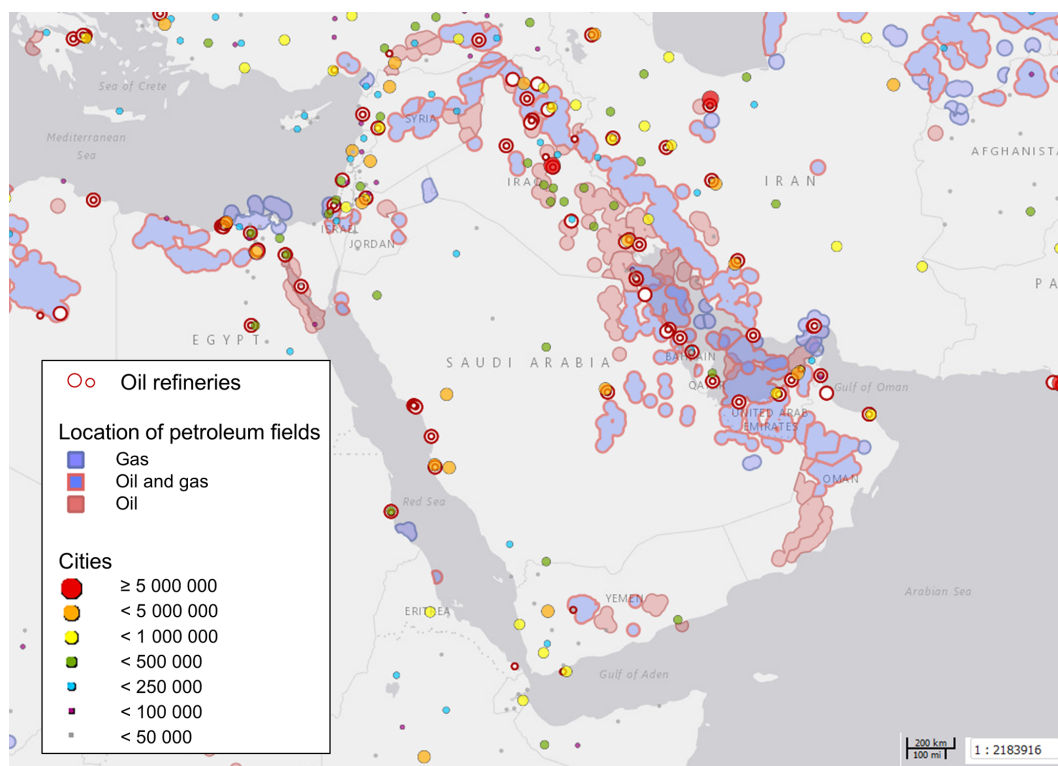
Figure 2. Oil refineries, petroleum fields and cities in the Arabian Basin. City markers are scaled with the number of inhabitants as denoted in the legend. Source: Harvard WorldMap Project (https://worldmap.harvard.edu/maps/6718/dJT, last access: 25 March 2019).

longer periods. Furthermore, a bias towards OVOCs in the assessment of speciated OH reactivity is also possible in this study because they were well covered by PTR-ToF-MS measurements, while longer-chain or branched alkenes and alkanes, which are components of oil and other fuels (D'Auria et al., 2009; Gueneron et al., 2015), were limited to C_2–C_8 compounds in the AQABA measurements. Nonetheless, considering the whole campaign, the Arabian Gulf was the region with the highest OH reactivity from alkanes (on average $\sim 1.2\,s^{-1}$ or $\sim 9\,\%$ of total OH reactivity). An important influence of oil and gas production on total OH reactivity in the Arabian Gulf is therefore evident in our data.

Petroleum extraction facilities and refineries are located at both shores of the Gulf of Suez and Suez Canal (Fig. 2), and wind from both east and west led to a relatively large contribution of alkanes (5 %–6 %; Fig. 1d, e).

By virtue of their double bond, alkenes are more reactive towards OH than alkanes. Indeed, in Saudi Arabian cities, OH reactivity of alkenes has been reported to be twice as high as the reactivity of alkanes, despite higher abundance of the latter (Barletta et al., 2017). Similarly, over the Arabian Gulf, the AQABA campaign results show an equivalent average share of OH reactivity from alkenes and alkanes (both $\sim 1.2\,s^{-1}$, which equals $\sim 9\,\%$), despite an ~ 11 times larger average mixing ratio of alkanes. Certainly a fraction of highly reactive alkenes emitted on land will have already

been oxidized before the emission-impacted air mass reached the point of observation on the ship. Alkene-attributed OH reactivity was slightly higher in the Suez Canal ($1.4\,s^{-1}$ vs. $1.2\,s^{-1}$), where the distance to emission sources is generally shorter due to the narrowness of the canal. Additionally, and probably more importantly, alkenes are only minor components in fossil fuel emissions generally. They are emitted from vehicle exhausts (a possible source near the Suez Canal) due to incomplete combustion (Koppmann, 2007). Alkanes, on the other hand, can be so abundant in emissions from oil and gas production that they dominate OH reactivity, as was observed in Colorado, where 60 % of OH reactivity calculated from VOC measurements (not total OH reactivity) was due to alkanes and only 8 % from alkenes (Gilman et al., 2013). In another study at the same site, alkanes contributed 26 %, alkenes 3 %, and aromatics 2 % of total OH reactivity (Swarthout et al., 2013). In contrast to that, alkenes (41 %) dominated over alkanes (23 %) in the OH reactivity calculated from VOC observations over Houston–Galveston Bay (Gilman et al., 2009).

Aromatics are important components of fossil fuels besides alkanes and alkenes (Koppmann, 2007). In Egyptian cities, ambient VOC mixing ratios from traffic have been reported to be dominated by aromatics (Matysik et al., 2010), whereas in Saudi Arabian cities, alkanes were more abundant (Barletta et al., 2017). Consistent with these findings, we ob-

served higher average speciated OH reactivity from aromatics ($1.3\,\mathrm{s}^{-1}$) in the Suez Canal (influenced by air from Cairo, roads next to the Suez Canal, a refinery, and a power plant) compared to the Arabian Gulf ($0.9\,\mathrm{s}^{-1}$, influenced by oil/gas industry emissions and partly by urban air from Saudi Arabia, Iraq and Kuwait).

A strong influence of maritime traffic in the narrow and highly frequented Suez Canal and Gulf of Suez is evident from the large NO_x contribution to total OH reactivity ($\sim$ 10 % and $\sim$ 12 %, respectively). Here, other vessels and their exhaust plumes passed by closely during waiting periods (before entering the Suez Canal in the northern Gulf of Suez and inside the Suez Canal).

The Arabian Gulf and Suez Canal will be discussed in more detail in case studies in Sect. 3.2.

3.1.2 Seaways influenced by maritime traffic: Red Sea, Gulf of Aden and Gulf of Oman

The Red Sea, the Gulf of Aden, and the Gulf of Oman displayed similar total OH reactivities with medians of 7.9–$8.5\,\mathrm{s}^{-1}$ during the AQABA campaign (northern Red Sea: median $8.5\,\mathrm{s}^{-1}$/mean $\pm$ standard deviation $9.1 \pm 3.3\,\mathrm{s}^{-1}$, southern Red Sea: $7.9\,\mathrm{s}^{-1}$/$8.7 \pm 4.2\,\mathrm{s}^{-1}$, Gulf of Aden: $8.0\,\mathrm{s}^{-1}$/$8.2 \pm 3.1\,\mathrm{s}^{-1}$, Gulf of Oman: $8.4\,\mathrm{s}^{-1}$/$8.4 \pm 3.1\,\mathrm{s}^{-1}$; also see Table 1 and Fig. 1c, d). These values are comparable to urban observations in the lower range, such as in Helsinki, Finland (Praplan et al., 2017), or Mainz, Germany (Sinha et al., 2008).

The OH reactivity over the Red Sea, Gulf of Aden and Gulf of Oman can largely be attributed to the influence of maritime transport in these busy, relatively constricted seaways. Refineries at the eastern shore of the northern Red Sea (Fig. 2) are not thought to have influenced our measurements due to prevailing wind from the northwest and west.

Among the three regions, the Gulf of Aden was the one with the lowest average total OH reactivity. Likely, this is due to its location in the transition zone to the open northwestern Indian Ocean (see Fig. 1c). Here, air masses were less influenced by pollution than over the Red Sea or Gulf of Oman, as the AQABA cruise took place during Northern Hemisphere summer, when the Intertropical Convergence Zone (ITCZ) is over India and comparably clean air is drawn north over the northwestern Indian Ocean (Ajith Joseph et al., 2018). In accordance with this finding, Bourtsoukidis et al. (2019) showed, by lifetime-variability regression of alkanes, that the Gulf of Aden was the area with the most remote character during AQABA.

In ship exhausts, the highest emission factors (apart from CO_2) have been found for NO_x (Endresen, 2003; Eyring, 2005; Huang et al., 2018). Large ship engines emit an average of 76 kg of NO_x per metric ton of fuel combusted (Eyring, 2005). This is reflected in the OH reactivity share of NO_x, which was in the range of 4 %–9 % in these relatively narrow seaway regions (Table 1). OVOCs accounted

for 12 %–21 % of total OH reactivity there, alkenes 4 %–9 %, inorganics (dominated by SO_2 and CO) 4 %–6 %, aromatics 3 %–8 % and alkanes 4 %–5 %. All those classes of compounds can stem from fuel combustion in ships (Endresen, 2003; Eyring, 2005; Huang et al., 2018; Xiao et al., 2018), which emit an average of 43 kg of SO_x, 4.7 kg of CO and 7 kg of hydrocarbons per metric ton of fuel combusted (Eyring, 2005).

The C_3 carbonyls (C_3H_6O) vs. propane (C_3H_8), C_5 oxidation products ($C_5H_{10}O$) vs. pentanes (C_5H_{12}) and toluene vs. benzene ratios (Table 1) were used here as indicators of the oxidation state (and, thereby, the extent of photochemical aging) of the air. We note that this approach is based on two assumptions: (1) that production of the carbonyls by oxidation dominates over direct emission, although some direct combustion emissions cannot be excluded, and (2) that the only carbonyl precursor is the corresponding C_3 or C_5 compound without significant fragmentation of larger VOCs. The toluene vs. benzene relationship is based on the assumption of simultaneous emission of both compounds. Notably, a distinct difference between the northern (less oxidized, $[C_3H_6O]/[C_3H_8] \approx 1.9$ and $[C_5H_{10}O]/[C_5H_{12}] \approx 1.3$) and southern Red Sea (oxidized, $[C_3H_6O]/[C_3H_8] \approx 9.4$ and $[C_5H_{10}O]/[C_5H_{12}] \approx 1.9$) was observed. Although it did not result in large differences in total OH reactivity values (median of $7.9\,\mathrm{s}^{-1}$ in the photochemically aged air masses in the south Red Sea and $8.5\,\mathrm{s}^{-1}$ in the north Red Sea), it reflects the origin of air masses: urban centers in northeast Africa for the north Red Sea, and the less populated and more distant Sudan and Chad for the south Red Sea.

3.1.3 Cleaner regions: Mediterranean and Arabian Sea

Over the more open seas, notably the Mediterranean and Arabian Sea (northwestern Indian Ocean), the air was aged, cleaner and less reactive to OH. Here, total OH reactivities were mostly close to the detection limit of $5.4\,\mathrm{s}^{-1}$. The median over the Mediterranean was $6.8\,\mathrm{s}^{-1}$ (average $\pm$ standard deviation: $7.2 \pm 2.9\,\mathrm{s}^{-1}$), which compares to the lower limits of observations from suburban areas such as Whiteface Mountain (Ren et al., 2006), Norfolk, UK (Ingham et al., 2009), central Pennsylvania (Ren et al., 2005), or El Arenosillo at the Spanish coast (Sinha et al., 2012) and more remote locations such as the Rocky Mountains (Nakashima et al., 2014). Total OH reactivity measured over the Arabian Sea during AQABA was, with a median of $4.9\,\mathrm{s}^{-1}$ (average $\pm$ standard deviation: $5.6 \pm 2.0\,\mathrm{s}^{-1}$), below the detection limit of $5.4\,\mathrm{s}^{-1}$. The marine OH reactivity calculated from trace gas measurements over the central Gulf of Mexico was $1.01\,\mathrm{s}^{-1}$ (Gilman et al., 2009), a value which was slightly exceeded in our observations over the open Arabian Sea with a speciated OH reactivity of $1.5 \pm 0.2\,\mathrm{s}^{-1}$.

Larger OH reactivity occurred over the Mediterranean Sea during short episodes of polluted air from the mainland in the Strait of Messina (between Sicily and Italy), vis-

ible in Fig. 1b. In the Strait of Messina and surroundings, total OH reactivity amounted to between $6.7 \pm 3.6\,\mathrm{s}^{-1}$ and $26.7 \pm 8.2\,\mathrm{s}^{-1}$ for 5 h, whereas before and after, it was close to the detection limit. OVOCs were with $\sim 11\,\%$–$12\,\%$ of total OH reactivity the largest group of identified OH sinks in both the Mediterranean and Arabian seas. Over the Mediterranean, the influence of shipping emissions was larger than over the Arabian Sea, evident from NO_x-attributed OH reactivity, which was on average $0.26\,\mathrm{s}^{-1}$ or $\sim 4\,\%$ of the total in the Mediterranean in contrast to $0.05\,\mathrm{s}^{-1}$ or $\sim 1\,\%$ of the total in the Arabian Sea. Johansson et al. (2017) found that ship traffic over the Arabian Sea causes $3\,\%$ of the global NO_x emissions from maritime transport, which explains why even here the conditions were not completely pristine.

3.2 Case studies

3.2.1 Arabian Gulf

Figure 1 shows the average OH reactivity composition for the Arabian Gulf. However, the air measured over the Arabian Gulf originated partly from Kuwait and/or Iraq, partly from Iran and partly from the south. The composition of total OH reactivity between the different regions of origin displayed distinct differences, and can therefore be divided according to origin of the measured air masses, shown in Fig. 3.

Notably, the air from Iraq and/or Kuwait showed obvious influence from oil extraction industries with large fractions of alkanes, alkenes and aromatics (Fig. 3). Here, emission sources were closest to the point of observation, which was reflected in the highest total OH reactivity (median: $18.8\,\mathrm{s}^{-1}$, average $\pm$ standard deviation: $18.7 \pm 7.9\,\mathrm{s}^{-1}$) and low C_3 carbonyls / propane and high toluene / benzene ratio medians of 0.3 and 0.8, respectively. In contrast, OH reactivity in the air originating from Iran was lower (median: $9.8\,\mathrm{s}^{-1}$, average $\pm$ standard deviation: $10.8 \pm 3.4\,\mathrm{s}^{-1}$), with a slightly higher C_3 carbonyls / propane and a lower toluene / benzene ratio (both 0.4). The OH reactivity here was similar to that found in air from the south (Saudi Arabia) with a median of $9.8\,\mathrm{s}^{-1}$ and a mean of $9.7 \pm 3.3\,\mathrm{s}^{-1}$; however, the C_3 carbonyls / propane ratio of 2.0 points to more oxidized air masses. The high OH reactivity in air originating from Kuwait and Iraq can be attributed to emissions from petrochemical extraction and processing industries that would explain the large contribution of alkanes, alkenes and aromatics. Apart from two notable exceptions, the distribution of OH reactivity did not differ significantly between air from Iran and the south. In air from Iran, the alkene fraction was larger than in air from the south, probably due to closer and different emission sources (gas extraction at the Iranian coast), which would also explain the lower C_3 carbonyls / propane ratio. The NO_x fraction was larger in air from the south, most likely for reasons of ship traffic influence.

Figure 4a depicts a time series of measurements along the ship track from entering the Arabian Gulf to Kuwait and back. The upper part of the graph shows indicators of the photochemical age of the air mass. The $[C_3H_6O]/[C_3H_8]$ ratio decreases and the toluene / benzene ratio increases when getting closer to Kuwait, meaning that the research vessel was approaching the emission sources (refineries, oil platforms). Both these indicators show opposite patterns, as expected. The $[C_5H_{10}O]/[C_5H_{12}]$ ratio follows the $[C_3H_6O]/[C_3H_8]$ ratio except for an increase towards Kuwait, which shows that the fresh emissions observed here were richer in propane than in pentanes and indicates a mix of fresh emissions with aged air masses. This observation will be discussed in more detail in Sect. 3.4.2. Changes in relative humidity indicate the varying influence of dry desert air and more humid air masses.

The following five case studies (orange numbered labels in Fig. 4 with corresponding air mass back trajectories) will go into more detail regarding the origin of OH reactivity (reported with $\pm 1\sigma$ total uncertainty) in the Arabian Gulf.

1. At the entrance to the Arabian Gulf after passing the Strait of Hormuz, total OH reactivity was comparably low ($8.0 \pm 4.0\,\mathrm{s}^{-1}$). Sampled air had traversed the open Indian Ocean, but passed over the Musandam Peninsula, where urban areas probably contributed some OH reactivity. OVOCs dominated ($36 \pm 20\,\%$ of OH reactivity), with an insignificant unattributed fraction of $38 \pm 76\,\%$.

2. At this location in the northern part of the Arabian Gulf, ca. 100 km from the coast of Saudi Arabia, total OH reactivity amounted to $22.1 \pm 7.2\,\mathrm{s}^{-1}$, mainly due to OVOCs ($57 \pm 29\,\%$), with large fractions of alkanes ($10 \pm 1\,\%$), alkenes ($16 \pm 8\,\%$) and aromatics ($10 \pm 5\,\%$). The back trajectories originate from eastern Iraq, with the urban areas of Amara and Basra. The large fraction of OVOCs is an indicator for chemically aged air. The aromatics, alkenes and alkanes were probably emitted from offshore oil/gas extraction platforms (Fig. 4b) and mixed with the oxidized air contaminants coming from a larger distance. Within the uncertainty of the measurement, there is no unattributed OH reactivity at this location; with values of $19.4 \pm 9.9\,\mathrm{s}^{-1}$ for the speciated OH reactivity and $22.1 \pm 7.2\,\mathrm{s}^{-1}$ for the measured total OH reactivity.

3. Approximately 30 km from the coast of Kuwait, the back trajectories indicate that the sampled air masses traveled over the Rumaila oil field in Basra (Iraq). Consequently, the total OH reactivity of $26.4 \pm 8.1\,\mathrm{s}^{-1}$ was mainly due to alkanes from oil extraction ($24 \pm 2\,\%$). In contrast to the previous case study, significant unattributed OH reactivity was observed here ($40 \pm 37\,\%$), which might be due to components of oil higher than C_8 and/or branched hydrocarbons that were not measured on board the *Kommandor Iona*.

4. Just after departure from the port of Kuwait, the highest observed OH reactivity ($32.8 \pm 9.6\,\mathrm{s}^{-1}$) of the cam-
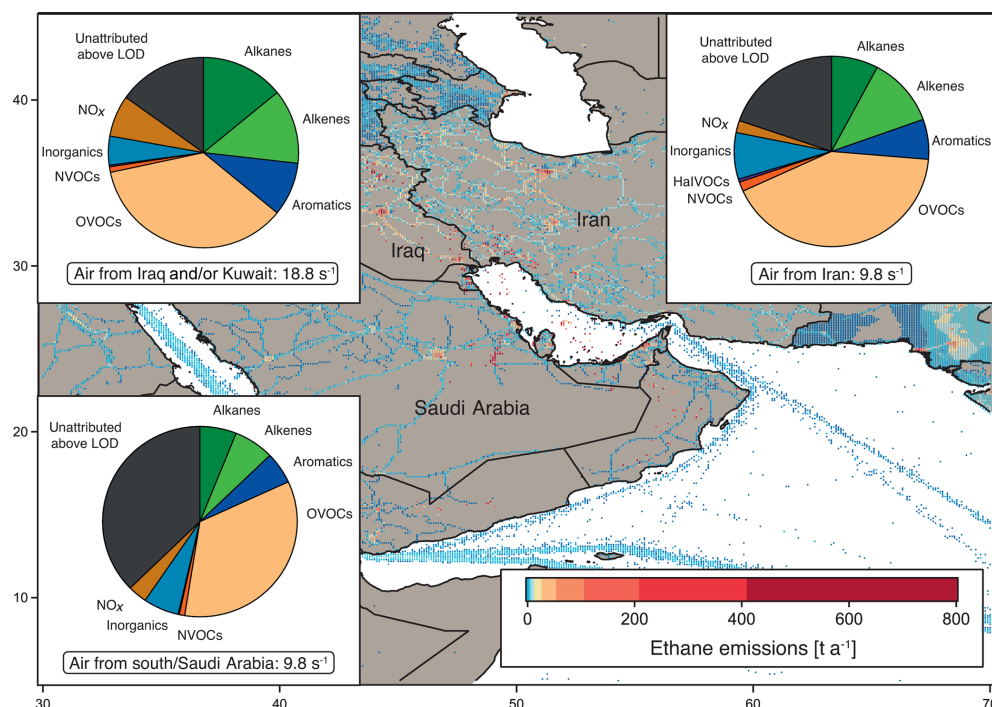
Figure 3. OH reactivity composition and average $\pm$ standard deviation in the Arabian Gulf, separated by origin of the measured air masses: from Iraq and/or Kuwait, from Iran and from southern Arabian Gulf and/or Saudi Arabia. Background: ethane emissions map using data from the EDGAR database (http://edgar.jrc.ec.europa.eu, last access: 31 August 2018, for 2012) as an indicator for the distribution of petroleum extraction and other anthropogenic sources.

paign was measured (except for refueling). HYSPLIT back trajectories show that it likely originated from large pollution sources at the coast: refineries (Saudi Aramco refinery and industrial area with storage tanks in Khafji, Saudi Arabia) and oil fields (Wafra oil field in Kuwait; oil platforms at the sea). Notably, alkenes ($23 \pm 14\%$) were a much larger OH sink here than alkanes ($5 \pm 0.5\%$), and the unattributed OH reactivity was zero within the uncertainty.

5. The largest OH reactivity measured during the whole campaign was $303.6 \pm 83.9\,\text{s}^{-1}$ during refueling of the vessel in front of the port of Fujairah (United Arab Emirates). A back trajectory would not be relevant here, as these are direct diesel fuel evaporation emissions, mainly composed of alkenes ($27 \pm 18\%$ of speciated OH reactivity) and aromatics ($21 \pm 10\%$), mixed with NO_x ($39 \pm 4\%$) from the bunker ship's own fuel combustion. Wu et al. (2015) measured total OH reactivity from gasoline evaporation with the CRM method. In their study, alkenes contributed 40% of measured OH reactivity, and they found an unattributed OH reactivity fraction of 43%. In our study, a larger percentage ($75 \pm 42\%$) of total OH reactivity remains unexplained in the fuel evaporation measurement, which is most likely due to the fact that fewer of the higher and branched hydrocarbons were measured.
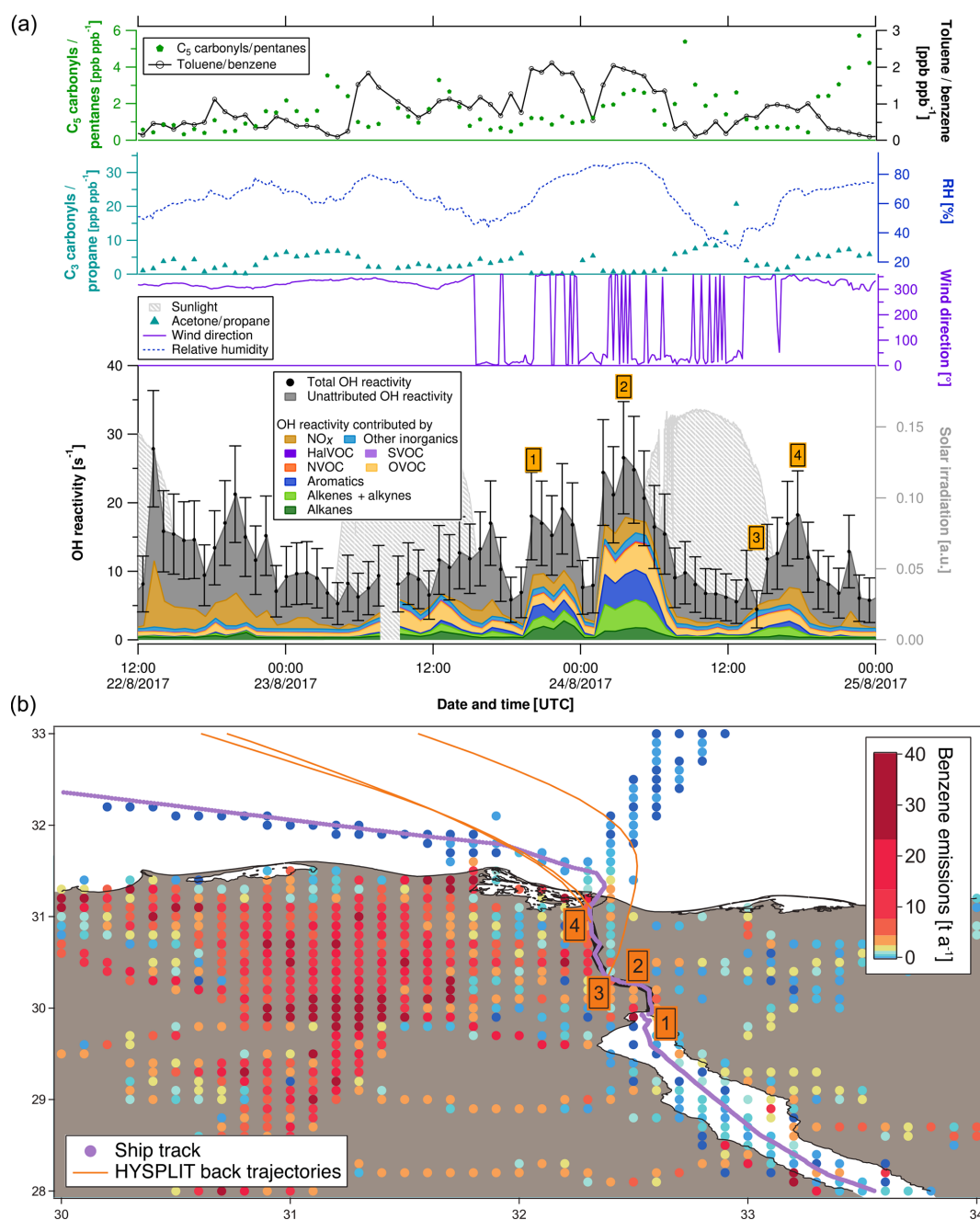
3.2.2 Suez Canal

The Suez Canal transit on 24 August 2017 was among the episodes of highest total OH reactivities during the whole campaign and will therefore be discussed in more detail here. In August 2017, 49 ships transited the Suez Canal per day (Suez Canal Authority, 2018). It is one of the world's most heavily used shipping lanes and there are no regulations concerning the fuel used or emission limitations. The Suez Canal is 193 km long and at the water surface 313 m wide (Suez Canal Authority, 2017). Given its narrowness, other vessels and their exhausts as well as urban areas or streets were relatively close to the *Kommandor Iona* while it was traveling along the Suez Canal. Consequently, variations in OH reactivity can mainly be attributed to local emissions. Therefore, back trajectories are usually not helpful for explaining OH reactivity over the Suez Canal.

Four case studies (orange numbered labels in Fig. 5) will elucidate the origin of OH reactivity (reported with $\pm 1\sigma$ total uncertainty) measured over the Suez Canal.

1. This 4 h period of higher OH reactivity (15.2 ± 5.8 to $19.1 \pm 6.6\,\text{s}^{-1}$) occurred during a waiting period at the southern entrance to the Suez Canal, in the port area of Suez City. Interestingly, OH reactivity was dominated by alkanes here ($\sim 10\%$–15%). This can be explained by the wind coming from north where directly at the
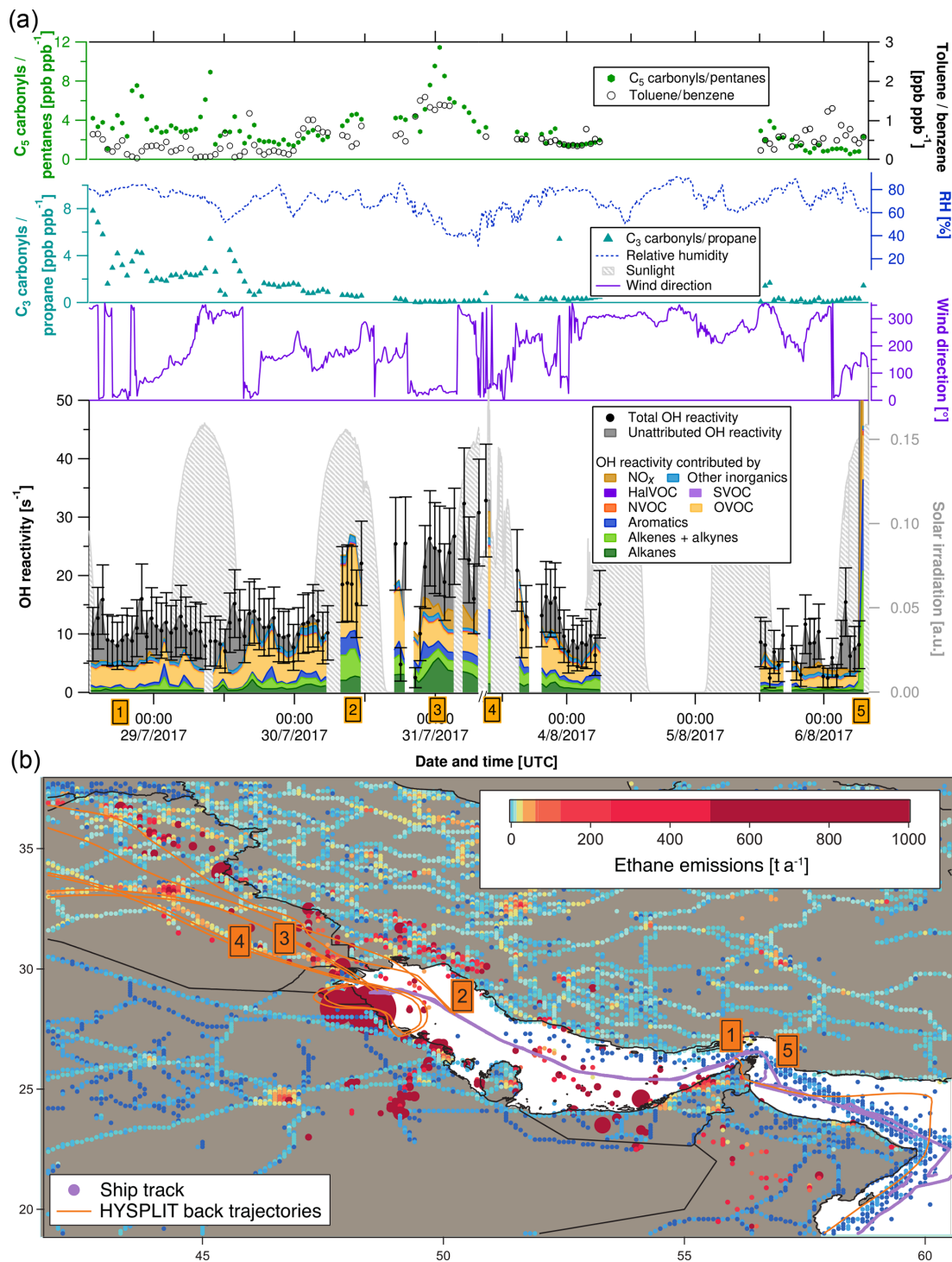
Figure 4. (a) C_3 carbonyls / propane ratio, C_5 carbonyls / pentane ratio, toluene / benzene ratio, relative humidity, solar irradiation, wind direction, speciated and measured OH reactivity in the Arabian Gulf. Error bars of total OH reactivity display the 1σ total uncertainty of the measurement. **(b)** Ship track of the campaign in the Arabian Gulf with HYSPLIT air mass back trajectories and numbered labels of case study points. Ethane emissions from the EDGAR database (http://edgar.jrc.europa.eu, last access: 31 August 2018, for 2012) as an indicator for petroleum extraction/processing and other anthropogenic sources are shown on a logarithmic color scale. Emissions out of scale ($> 1000\,\mathrm{t\,a^{-1}}$) are shown with larger circles.

Figure 5. (a) C_3 carbonyls / propane ratio, C_5 carbonyls / pentane ratio, toluene / benzene ratio, relative humidity, solar irradiation, wind direction, speciated and measured OH reactivity in the Suez Canal. Error bars of total OH reactivity display the total uncertainty of the measurement. **(b)** Ship track of the cruise in the Suez Canal with HYSPLIT air mass back trajectories and numbered labels of case study points. Benzene emissions as an indicator for anthropogenic sources from the EDGAR database (http://edgar.jrc.ec.europa.eu, last access: 31 August 2018, for 2012) are shown on a logarithmic color scale.

shore a petrol storage area is located (Nasr Petroleum Company, Suez, Egypt). The toluene / benzene ratio was between 1 and 3, indicating fuel combustion emissions as a source in Suez City and/or from ships, rather than biomass burning, which tends to be richer in benzene.

2. The Great Bitter Lake is part of the Suez Canal and is used by ships as a "passing lane". During the 4 h waiting time in the lake, the highest OH reactivity of the transit was observed (20.6 ± 6.9 to $26.6 \pm 8.2\,\mathrm{s^{-1}}$). Alkenes, aromatics and OVOCs contributed almost equally to this value ($\sim 16\,\%$, $\sim 17\,\%$, and $\sim 17\,\%$, respectively).

In particular, the large amount of aromatics is notable. With $7 \pm 1\%$ contribution, alkanes were less relevant here than in the Suez City port (case study 1). A visible source of nearby emissions at the northern lakeshore (with northerly winds) was a power plant running on natural gas and/or heavy fuel oil (Abu Sultan Power Station, Ismailia, Egypt (Global Energy Observatory, 2015). Its emissions may have been mixed with those from the lakeshore settlements and from bypassing cargo ships, with a toluene / benzene ratio between 1 and 3, characteristic for fuel combustion emissions.

3. This point of observation was low in OH reactivity $(5.5 \pm 3.2\,\mathrm{s}^{-1})$ as well as in relative humidity (29.2%). Combined with the back trajectory, this indicates that the air mass sampled here had passed over the Sinai Desert. In this location, the C_3 carbonyls / propane ratio was 20.7, indicating a photochemically aged air mass. For comparison, the ratio was never above 10 anywhere else in the area, and in case studies 1 and 2 even between 0 and 1. Similarly, the C_5 carbonyls / pentanes ratio was elevated (2.6) and the toluene / benzene ratio was low (0.5).

4. The wind direction at case study point 4 was north-northwest. Total OH reactivity was in a 4 h peak of 11.8 ± 5.0 to $18.2 \pm 6.4\,\mathrm{s}^{-1}$. Circa 15 % of it was caused by NO_x and $\sim 9\%$ by alkenes. The toluene / benzene ratio was ~ 1, which indicates a fuel combustion source. There is a highway located west of this northern part of the Suez Canal (Ismailia-Port Said Road), but given the wind direction, exhaust plumes of other vessels sailing in front of the research ship were probably relevant for the OH reactivity as well as traffic on land.

3.3　How many and which chemical species contribute to total OH reactivity around the Arabian Peninsula?

Many studies of ambient total OH reactivity show significant unattributed or missing OH reactivity (Yang et al., 2016). Care must be taken in interpreting this missing fraction as it depends on which individual compounds are taken into account, although forest studies have tended to show greater missing reactivity fractions than urban studies (Williams and Brune, 2015). Using a total of 120 chemical species (listed in Table S1), we calculated the speciated OH reactivity in 50 min time resolution for the whole AQABA campaign. For the data points with speciated OH reactivity above the CRM detection limit, the unattributed fraction of total OH reactivity is plotted against the number of compounds taken into account in Fig. 6. Only data points above the detection limit were chosen in order to exclude seemingly unattributed OH reactivity which is actually due to the detection limit (unattributed fractions for all data points are shown along with those for above the LOD in Table 1). The graph
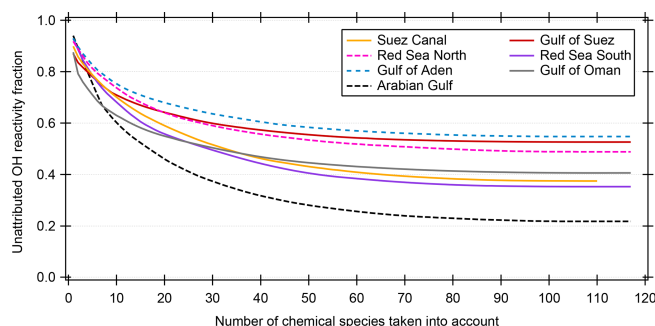

Figure 6. Unattributed OH reactivity fraction as a function of the number of compounds/chemical species taken into account for calculating speciated OH reactivity. The chemical species are taken into account with decreasing average OH reactivity. Only data points where the summed speciated OH reactivity is larger than or equal to the detection limit (LOD) of the CRM measurement are considered here. The Mediterranean and Arabian seas are not shown because of insignificant number of data points above the LOD.

shows that when up to ca. 100 species are considered, the unattributed OH reactivity fraction decreases. The remaining compounds collectively contribute only minor additional OH reactivity (less than $0.012\,\mathrm{s}^{-1}$). Total OH reactivity is best explained by measured trace gases in the Arabian Gulf ($22 \pm 56\%$ unattributed), in the Suez Canal and southern Red Sea ($37 \pm 34\%$ and $35 \pm 55\%$ unattributed, respectively). The largest unattributed OH reactivity was found in the Gulf of Aden ($55 \pm 38\%$). Other regions with significant unattributed fractions were the northern Red Sea ($49 \pm 39\%$) and the Gulf of Suez ($53 \pm 35\%$). The unattributed reactivity fraction does not correlate with the indicators used for estimating the air mass age.

Figure 7 shows the average OH reactivity of VOCs by molecular mass (NO_x and other inorganic compounds are not considered in this graph) and color-coded for groups of compounds for the Arabian Gulf and the Suez Canal. Higher-mass aromatics play a larger role in the Suez Canal while the same OVOCs are important in both regions. Generally, fewer VOCs in the higher mass ranges were measured, which is likely due to larger molecules being partially lost in the ca. 10 m long, 50 °C inlet line. This means that some less volatile components of total OH reactivity might have been missed in this setup. As the same inlet was used for VOC and OH reactivity measurements, however, this does not impact the unattributed reactivity fraction.

The 10 chemical species which contributed most to OH reactivity in each region traversed during the AQABA campaign are displayed in Fig. 8. Generally, in no regional average was one single compound responsible for an OH reactivity of more than $1.4\,\mathrm{s}^{-1}$. This reflects the previous discussion highlighting the necessity of considering a large number of species to get a complete picture of total OH reactivity. The concentrations of some of the compounds among the 10 most
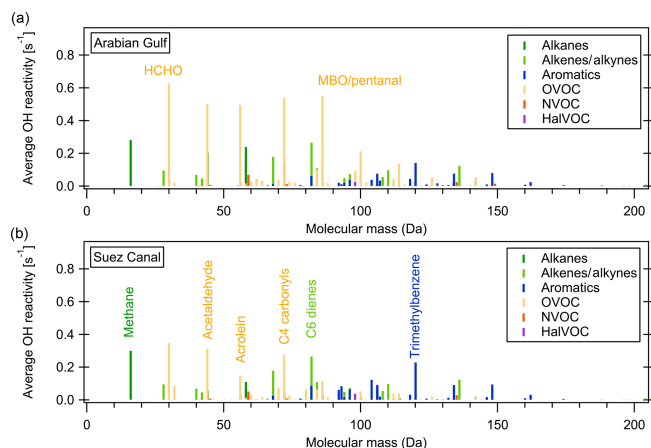
Figure 7. Average OH reactivity of VOCs by molecular mass in the Suez Canal and Arabian Gulf. Colors show the compound class.

relevant ones were derived with the theoretical approach (see Sect. 2.5) and therefore have larger uncertainties. However, their potential importance underlines that a focus on the 14 compounds calibrated with a typical PTR−MS gas standard would not be sufficient for a comprehensive understanding of OH reactivity. Overall, the contribution of the 78 species derived by the theoretical approach amounts to between 22 % (Gulf of Suez) and 51 % (southern Red Sea) of speciated OH reactivity (see Table 1).

The highest percentage contribution to total OH reactivity by the 10 most important compounds was seen in the Gulf of Oman (39±20 %) and the Arabian Gulf (38±20 %), amongst which were the four theoretically calibrated exact masses of acrolein, MBO and/or pentanal, C_4 carbonyls and C_6 dienes.

The importance of the seaways around the Arabian Peninsula for maritime transport is reflected in the large contribution of NO_2 and CO (associated with fuel combustion), which are among the three highest contributors to OH reactivity in most of the regions and among the top 10 in all of them. Oxygenated species such as aldehydes and ketones were important OH sinks in all the areas, in particular formaldehyde, acetaldehyde and, to a lesser extent, the C_4 and C_5 carbonyls. Directly emitted hydrocarbons were among the 10 most important OH reactivity contributors only in areas closer to emission sources: e.g., *n*-butane and propane in the Gulf of Suez, or unsaturated hydrocarbons such as C_6 dienes, C_5 dienes (without isoprene) and ethene in the Suez Canal. The importance of oxygenates in the air composition during AQABA reflects the fast photooxidation of direct emissions during this summertime campaign (also see Sect. 3.1.1). In winter, the directly emitted hydrocarbons would have longer lifetimes and therefore gain importance in the OH reactivity budget at the expense of oxygenates.

In the Arabian Sea, which was the area with the lowest total OH reactivities (Fig. 1, Table 1), the global background OH reactivity from methane was a major OH sink. Dimethyl

sulfide (DMS), a biogenic molecule emitted by algae which has been observed in this part of the ocean before (Warneke and Gouw, 2001) and will be discussed elsewhere for the AQABA campaign (Edtbauer et al., 2019), appears among the 10 most important OH sinks here despite a reactivity of only $0.02\,s^{-1}$. This is evidence for relatively clean air due to the influence of open ocean air, although even here emissions from shipping are evident from the CO and NO_2 contributions. In the Mediterranean, methane was the second most important single contributor to total OH reactivity after CO.

Generally, anthropogenic VOCs and their oxidation products dominated OH reactivity around the Arabian Peninsula. For example, acrolein was among the 10 most important contributors almost everywhere during AQABA (Fig. 8). Acrolein is a major product of the oxidation of 1,3-butadiene, which is among the most abundant alkenes emitted from anthropogenic sources (Grosjean et al., 1994). The C_4 carbonyls (butanal or methyl ethyl ketone, MEK), are major contributors to total OH reactivity over the Arabian Basin, and both can be directly emitted from fossil fuel combustion (Schauer et al., 2002) or be the result of ambient oxidation processes. Carbonyl photolysis has been found recently to be a possible source of ozone formation in an oil and gas production area (Edwards et al., 2014).

3.4 OH reactivity and ozone

3.4.1 Ozone production regimes

Ozone and OH reactivity are connected via a chemical cycle that involves NO_x and VOCs (Sillman, 1999; Ren et al., 2013): OH oxidizes VOCs to form peroxy radicals, which, in turn, oxidize NO to NO_2. NO_2 thus formed is subsequently photolyzed to result in ozone production. Ozone formation is, however, neither linearly dependent on NO_x concentration nor VOC reactivity, and a decrease in one parameter does not necessarily lead to a decrease in ozone formation (Pusede and Cohen, 2012).

Defining ozone production regimes in terms of the OH reactivities of VOCs and NO_x is a way of assessing the sensitivity of ozone production to the prevailing conditions (Kirchner et al., 2001; Sinha et al., 2012). The method and underlying chemistry have been extensively evaluated for different conditions and compared to other methods in Kirchner et al. (2001). The amount of peroxy radicals produced by VOC oxidation is linked to the OH reactivity of VOCs. The OH reactivity of VOCs was calculated here as the difference of measured total OH reactivity (in 5 min time resolution) and OH reactivity of measured NO_x. Only data in the daytime (06:00–18:00 local time) were considered because the method is inherently limited to daytime chemistry. Figure 9 shows ozone production regime plot examples, where "*s*" denotes the relative reactivity of OH towards NO_x and VOCs. Based on the analysis of Kirchner et al. (2001), which was developed for urban VOC mixtures, in between the lines la-
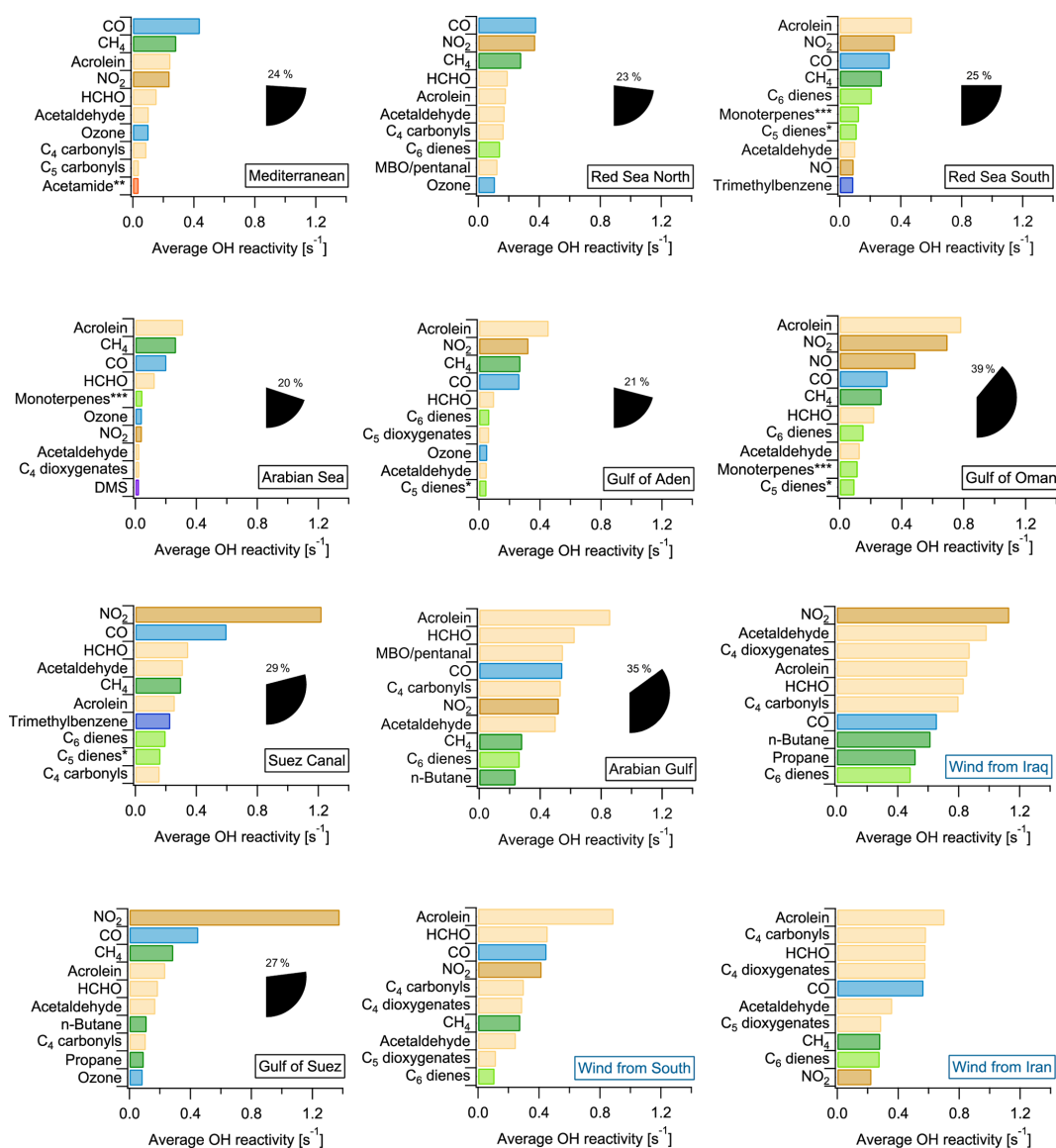
Figure 8. Regional average OH reactivity of each of the 10 most important contributors to OH reactivity. The percentage of total OH reactivity from these 10 compounds is shown as pie wedges. The Arabian Gulf was split by air mass origin (plots with blue labels). * C_5 dienes do not include isoprene. ** Acetamide or N-methyl formamide. *** "Monoterpenes" may include anthropogenic C_{10} trienes. MBO: 2-methyl-3-buten-2-ol.

beled $s = 0.2$ and $s = 0.01$, ozone production is favored by a suitable ratio of NO_x and OH reactivity of VOCs, whereas $s > 0.2$ indicates VOC limitation, and $s < 0.01$ NO_x limitation. The Arabian Sea with its comparably clean air was a region with partially NO_x-limited ozone production (Fig. 9a). Here, 20 % of the data points do not fall within the regime of ozone production, mostly due to NO_x limitation. This is reflected in relatively low ozone mixing ratios. The Gulf of Suez (Fig. 9b) is characterized in part by a strong VOC limitation associated with high NO_x (69 % of data points indicate an ozone formation regime). This NO_x can be attributed to emissions from other vessels at close proximity while wait-

ing at the entrance of the Suez Canal. The low ozone mixing ratios associated with high NO_x in the fresh combustion emissions (Fig. 9b, c) point to ozone titration, which will be discussed in greater detail in Sect. 3.4.2. In the Suez Canal (Fig. 9c), the data points are also grouped more towards VOC sensitivity whereas the opposite is true for the Arabian Gulf (Fig. 9d). Nevertheless, in both the Suez Canal and the Arabian Gulf, almost all data points (97 % in the Arabian Gulf and 91 % in the Suez Canal) fall into the regime of ozone formation, meaning that a suitable ratio of VOC and NO_x molecules for ozone formation was present nearly all the time. The same is true for the other environments (not shown
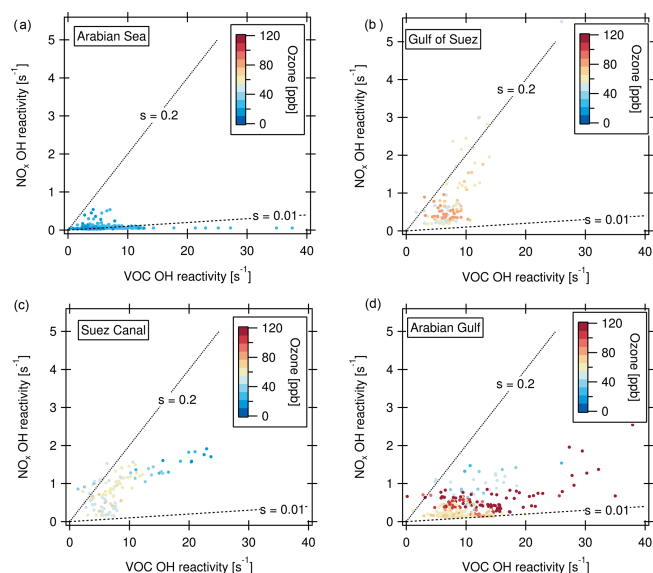
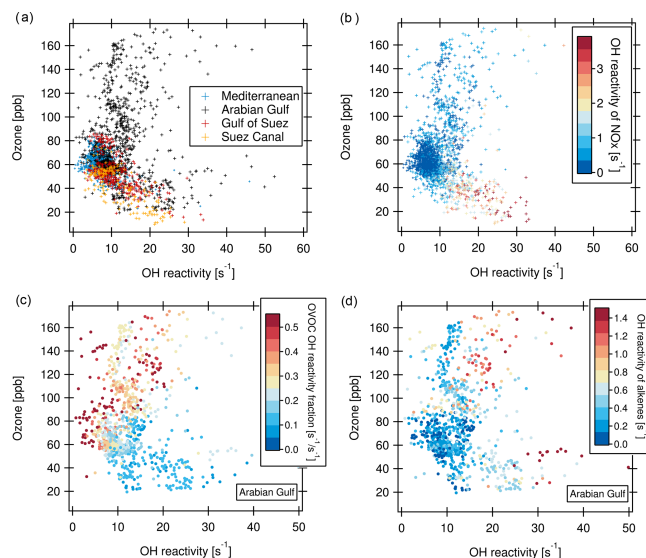**Figure 9.** Ozone production regimes for the **(a)** Arabian Sea, **(b)** Gulf of Suez **(c)** Suez Canal and **(d)** Arabian Gulf. "s" denotes the relative reactivity of OH towards NO_x and VOCs. $s > 0.2$: VOC limitation; $s < 0.01$: NO_x limitation of the ozone formation.

Figure 10. (a) Ozone vs. total OH reactivity for four regions. **(b)** Same as **(a)**, but with OH reactivity of NO_x as color scale (no data points when NO_x values are missing). **(c)** Ozone vs. OH reactivity for the Arabian Gulf with the fraction of OVOC in total OH reactivity as color scale. **(d)** Ozone vs. OH reactivity for the Arabian Gulf with OH reactivity of alkenes as color scale.

in graph) with favored ozone formation 97 % of the time in the Mediterranean, 93 % in the northern Red Sea, 88 % in the southern Red Sea, 87 % in the Gulf of Aden and 82 % in the Gulf of Oman.

The ozone production favoring conditions with both high NO_x- and VOC-attributed OH reactivities may be contributing factors to the high ozone levels observed and modeled above the Arabian Gulf (Lelieveld et al., 2009; Fountoukis et al., 2018). Conditions favorable for ozone formation resulting in ozone mixing ratios up to 14 ppb have been reported from other sites influenced by oil and gas production (Edwards et al., 2014; Wei et al., 2014). Moradzadeh et al. (2019) found that a hydrocarbon processing plant at the shore of the Arabian Gulf impacted ozone levels even at a 300 km distance. Generally, emissions in lower latitudes (e.g., below 30° N as in the Arabian Gulf) lead to more efficient formation of tropospheric ozone than in higher latitudes because the meteorological conditions lead to faster reaction rates and strong convection (Zhang et al., 2016).

3.4.2 OH reactivity/ozone correlations

The relationship between ozone and total OH reactivity during the AQABA campaign is depicted in Fig. 10. Data from most regions display a negative correlation between ozone mixing ratio and total OH reactivity. This is exemplified for the Mediterranean, Suez Canal and Gulf of Suez in Fig. 10a (correlation for Suez Canal: slope $= -0.2$; $r^2 = 0.61$). Additionally, there is a large group of data points located at lower OH reactivity (below $10\,s^{-1}$) and ozone mixing ratios of 50 to 70 ppb.

The reason for the negative correlation seen in parts of the data is displayed in Fig. 10b. Higher OH reactivities in this part of the plot coincide with higher NO_x, stemming from the exhaust plumes of vessels passing close by. In these ship plumes, high levels of VOCs are co-emitted with NO_x. This combination leads to elevated total OH reactivity. At the same time, ozone is depleted by the NO emissions in the fresh ship plumes ($NO + O_3 \rightarrow NO_2 + O_2$, Sillman, 1999). This effect is seen when an emission source co-emitting NO_x and VOCs is very close (Akimoto, 2016), as ozone values recover rapidly downwind through NO_2 photolysis and mixing. The ozone titration effect has similarly been observed in negative ozone–CO correlations (Parrish et al., 1998).

The bulk of data points between 50 and 70 ppb of ozone associated with lower OH reactivity and no trend are, on the other hand, more representative of a campaign background/average, uninfluenced by immediate emission sources and with lower NO_x (Fig. 10b). Here, a possible longer-term effect of the co-emission of VOC and NO_x from marine transport and other anthropogenic sources can be seen. As a secondary pollutant and being suppressed by NO, ozone can often be elevated at a distance from the pollution sources (Sudo and Akimoto, 2007). Large quantities of ozone can be produced during long-range transport under sunlight influence (Parrish et al., 1998; Akimoto, 2016; Moradzadeh et al., 2019). Consequently, in the seaways around the Arabian Peninsula, ozone mixing ratios were mostly between 50 and 80 ppb, which is the range of daytime values in polluted Beijing (Williams et al., 2016; Yang et al., 2017).

Over the Arabian Gulf, the same negative relationship between OH reactivity and ozone as in the Suez Canal, Gulf of Suez and Mediterranean existed in those data points where ozone was below 70 ppb. In contrast, at ozone mixing ratios above ca. 80 ppb, no trend or a slightly positive correlation between ozone mixing ratio and OH reactivity can be ascertained (Fig. 10a). Ozone mixing ratios above 70 ppb over the Arabian Gulf were associated with a high fraction of OVOCs (Fig. 10c), indicating more photochemically processed air. Additionally, when OH reactivity was high at the same time as ozone, alkene OH reactivity was also elevated (Fig. 10d). This points to a mixing of fresh emissions (associated with short-lived alkenes) into photochemically aged, oxidized air contaminants (high OVOCs and high ozone) over the Arabian Gulf. Polluted air masses from urban or industrial areas on land were probably oxidized during their transport to the coast/sea, where they were mixed with emissions from oil and gas extraction facilities, as has been discussed in detailed case studies of such occasions in Sect. 3.2.

4   Summary and conclusions

In July and August 2017, during the AQABA campaign, the first ship-based direct measurements of total OH reactivity were conducted using the comparative reactivity method. The total OH reactivity in ambient air around the Arabian Peninsula was predominantly related to anthropogenic influence. In particular, reactive hydrocarbons from oil and gas extraction/production and inorganic reactants such as NO_x and CO from fuel combustion by shipping were major OH sinks during the whole campaign. Total OH reactivity over the Arabian Basin varied, with periods below the detection limit over the Arabian Sea, regional medians of 7.9–$8.5\,s^{-1}$ under permanent maritime traffic influence over the seaways of the Red Sea, Gulf of Aden and Gulf of Oman, and episodes of up to $32.8 \pm 9.6\,s^{-1}$ when air masses were influenced by emissions from oil/gas extraction facilities, urban centers and/or ships in close proximity. The largest regional median OH loss rate of $18.8\,s^{-1}$ was observed over the Arabian Gulf when air originated from Iraq and/or Kuwait, where large oil fields and refineries at the shore provided high emissions. Over the Suez Canal, median OH reactivities of 10.8 and up to $26.6 \pm 8.2\,s^{-1}$ were attributed to local emissions from a petroleum storage facility, a power plant, and traffic on sea and land. The cleanest environment was the Arabian Sea, where the marine biogenic compound dimethyl sulfide was among the 10 most important known contributors to OH reactivity.

In all the regions around the Arabian Peninsula, OVOCs were the class of compounds that provided the largest identified OH sink. They were formed efficiently because photochemistry was highly active due to intense solar irradiation and high temperatures in summer. Photochemically aged air mixed with fresh nearby emissions over the Arabian Gulf,

leading to extremely high ozone mixing ratios. Using ozone production regime plots, we found that the ratio of VOC- and NO_x-attributed OH reactivities was favorable for ozone formation nearly all along the ship track. In the Arabian Gulf, large OH reactivity from VOCs due to oil and gas sources together with NO_x from marine traffic lead to a regime of ozone production 97 % of the time. The only regions where ozone production was limited for a significant fraction of time were the Gulf of Suez with VOC limitation when affected by NO_x-rich plumes, and the Arabian Sea with a slight NO_x limitation due to clean air from the open Indian Ocean. Ozone versus OH reactivity correlation plots were found to be a valuable tool in identifying different chemical regimes with regards to ozone formation and loss: ozone destruction in NO_x-rich ship plumes was clearly distinguishable from a mix of fresh petroleum extraction emissions with photochemically aged air.

Studies of ambient total OH reactivity often show a significant missing or unattributed fraction of OH reactivity, although this tends to be smaller in anthropogenic environments (Williams and Brune, 2015). In an attempt to close the OH reactivity budget, the OH reactivity of compounds with unidentified structure from PTR-ToF-MS measurements was calculated using averages of the reaction rate constants of all possible structures attributed to each chemical formula. These species were important OH sinks, accounting for 22 %–51 % of the regional speciated OH reactivity. With this approach, the measured total OH reactivity can be explained within the uncertainty for the Suez Canal, the southern Red Sea, the Gulf of Oman and the Arabian Gulf. Significant unattributed fractions remain in the Gulf of Suez, the northern Red Sea and the Gulf of Aden. Overall, ~ 100 chemical species needed to be identified to explain the measured total OH reactivity within the uncertainty, while the 10 most important compounds contributed 20 %–39 % of the reactivity. Unattributed reactivity in plumes from hydrocarbon processing facilities may be due to branched and/or higher hydrocarbons not captured with the techniques available on board the *Kommandor Iona*. In order to get a more comprehensive picture of the chemical species relevant for OH chemistry in the region, measurements with even greater chemical detail in the hydrocarbons would be necessary.

The range and composition of OH reactivity (and the ozone mixing ratios) around the Arabian Peninsula were, despite the marine measurement locations, broadly comparable to observations from highly populated urban areas, except for an unusually large contribution of OVOCs (Kovacs et al., 2003; Mao et al., 2010; Dolgorouky et al., 2012; Kim et al., 2016; Williams et al., 2016; Praplan et al., 2017; Yang et al., 2017). The "urban-like" OH reactivity is related to intensive international ship traffic in the seaways in the Arabian Basin and to major emissions from oil and gas industries on sea platforms and at the coasts. Oil- and gas-related VOCs were important sources of OH reactivity, and could be a relevant factor for the extremely high ozone concentrations and the

photochemical air pollution usually seen in summer in the region (Lelieveld et al., 2009; Smoydzin et al., 2012; Farahat, 2016; Barkley et al., 2017).

Most predictions assume that oil and natural gas production will increase in the Middle East during the coming decades (Balat, 2006; Khatib, 2014; Holz et al., 2015; Overland, 2015). Similarly, ship emissions around the Arabian Peninsula have been projected to grow in the short term due to intensifying traffic (Eyring et al., 2007), although new emission regulations set by the International Maritime Organization (IMO, 2019), effective from 2020, might lead to a long-term decrease. Given that the conditions favor ozone production and will increasingly do so due to rising temperatures (Wasimi, 2010; Lelieveld et al., 2012, 2016), emission regulations in the region appear to be the only way to prevent a further increase in photochemical air pollution in the future.

Author contributions. EP and NW were responsible for OH reactivity measurements and data. EP conducted further data analysis and wrote the first draft of the paper. AE, EB, LE and CS contributed VOC and NMHC measurements and data. Ozone and SO_2 data were provided by JC and PE, formaldehyde and NO_x data by DD, BH, IT, and HF, and methane and carbon monoxide by JP. DW calculated the back trajectories. JL designed and realized the campaign. JW supervised the study. All authors contributed to paper writing and revision and read and approved the submitted version.

References

Abdelkader, M., Metzger, S., Mamouri, R. E., Astitha, M., Barrie, L., Levin, Z., and Lelieveld, J.: Dust–air pollution dynamics over the eastern Mediterranean, Atmos. Chem. Phys., 15, 9173–9189, https://doi.org/10.5194/acp-15-9173-2015, 2015.

Ajith Joseph, K., Jayaram, C., Nair, A., George, M. S., Balchand, A. N., and Pettersson, L. H.: Remote Sensing of Upwelling in the Arabian Sea and Adjacent Near-Coastal Regions, in: Remote Sensing of the Asian Seas, 1st edition 2019, edited by: Barale, V. and Gade, M., Springer International Publishing, Cham, 467–483, 2018.

Akimoto, H.: Tropospheric Reaction Chemistry, in: Atmospheric Reaction Chemistry, Springer Japan, Tokyo, 285–386, 2016.

Balat, M.: The Position of Oil in the Middle East: Potential Trends, Future Perspectives, Market and Trade, Energ. Source. Part A, 28, 821–828, https://doi.org/10.1080/009083190951384, 2006.

Barkley, M. P., González Abad, G., Kurosu, T. P., Spurr, R., Torbatian, S., and Lerot, C.: OMI air-quality monitoring over the Middle East, Atmos. Chem. Phys., 17, 4687–4709, https://doi.org/10.5194/acp-17-4687-2017, 2017.

Barletta, B., Simpson, I. J., Blake, N. J., Meinardi, S., Emmons, L. K., Aburizaiza, O. S., Siddique, A., Zeb, J., Yu, L. E., Khwaja, H. A., Farrukh, M. A., and Blake, D. R.: Characterization of carbon monoxide, methane and nonmethane hydrocarbons in emerging cities of Saudi Arabia and Pakistan and in Singapore, J. Atmos. Chem., 74, 87–113, https://doi.org/10.1007/s10874-016-9343-7, 2017.

Boersma, K. F., Vinken, G. C. M., and Tournadre, J.: Ships going slow in reducing their NOx emissions: Changes in 2005–2012 ship exhaust inferred from satellite measurements over Europe, Environ. Res. Lett., 10, 74007, https://doi.org/10.1088/1748-9326/10/7/074007, 2015.

Bourtsoukidis, E., Ernle, L., Crowley, J. N., Lelieveld, J., Paris, J.-D., Pozzer, A., Walter, D., and Williams, J.: Non-methane hydrocarbon (C_2–C_8) sources and sinks around the Arabian Peninsula, Atmos. Chem. Phys., 19, 7209–7232, https://doi.org/10.5194/acp-19-7209-2019, 2019.

Buzcu, B. and Fraser, M. P.: Source identification and apportionment of volatile organic compounds in Houston, TX, Atmos. Environ., 40, 2385–2400, https://doi.org/10.1016/j.atmosenv.2005.12.020, 2006.

Chenoweth, J., Hadjinicolaou, P., Bruggeman, A., Lelieveld, J., Levin, Z., Lange, M. A., Xoplaki, E., and Hadjikakou, M.: Impact of climate change on the water resources of the eastern Mediterranean and Middle East region: Modeled 21st cen-

tury changes and implications, Water Resour. Res., 47, W06506, https://doi.org/10.1029/2010WR010269, 2011.

Cook, B. I., Anchukaitis, K. J., Touchan, R., Meko, D. M., and Cook, E. R.: Spatiotemporal drought variability in the Mediterranean over the last 900 years, J. Geophys. Res.-Atmos., 121, 2060–2074, https://doi.org/10.1002/2015JD023929, 2016.

D'Auria, M., Emanuele, L., Racioppi, R., and Velluzzi, V.: Photochemical degradation of crude oil: Comparison between direct irradiation, photocatalysis, and photocatalysis on zeolite, J. Hazard. Mater., 164, 32–38, https://doi.org/10.1016/j.jhazmat.2008.07.111, 2009.

Dolgorouky, C., Gros, V., Sarda-Esteve, R., Sinha, V., Williams, J., Marchand, N., Sauvage, S., Poulain, L., Sciare, J., and Bonsang, B.: Total OH reactivity measurements in Paris during the 2010 MEGAPOLI winter campaign, Atmos. Chem. Phys., 12, 9593–9612, https://doi.org/10.5194/acp-12-9593-2012, 2012.

Donat, M. G., Peterson, T. C., Brunet, M., King, A. D., Almazroui, M., Kolli, R. K., Boucherf, D., Al-Mulla, A. Y., Nour, A. Y., Aly, A. A., Nada, T. A. A., Semawi, M. M., Al Dashti, H. A., Salhab, T. G., El Fadli, K. I., Muftah, M. K., Dah Eida, S., Badi, W., Driouech, F., El Rhaz, K., Abubaker, M. J. Y., Ghulam, A. S., Erayah, A. S., Mansour, M. B., Alabdouli, W. O., Al Dhanhani, J. S., and Al Shekaili, M. N.: Changes in extreme temperature and precipitation in the Arab region: long-term trends and variability related to ENSO and NAO, Int. J. Climatol., 34, 581–592, https://doi.org/10.1002/joc.3707, 2014.

Doskey, P. V., Fukui, Y., Sultan, M., Al Maghraby, A., and Taher, A.: Source Profiles for Nonmethane Organic Compounds in the Atmosphere of Cairo, Egypt, J. Air Waste Manage., 49, 814–822, https://doi.org/10.1080/10473289.1999.10463850, 1999.

Draxler, R. R. and Hess, G. D.: An Overview of the HYSPLIT_4 Modelling System for Trajectories, Dispersion, and Deposition, Aust. Meteorol. Mag., 47, 295–308, 1998.

Edtbauer, A., Stönner, Christof, Berasategui, M., Walter, D., Crowley, J., Lelieveld, J., and Williams, J.: Measurements of DMS, DMSO2 and a new marine biogenic emission, methane sulfonamide (MSAM) in air over the Arabian Sea, mansucript in preparation, 2019.

Edwards, P. M., Brown, S. S., Roberts, J. M., Ahmadov, R., Banta, R. M., deGouw, J. A., Dubé, W. P., Field, R. A., Flynn, J. H., Gilman, J. B., Graus, M., Helmig, D., Koss, A., Langford, A. O., Lefer, B. L., Lerner, B. M., Li, R., Li, S.-M., McKeen, S. A., Murphy, S. M., Parrish, D. D., Senff, C. J., Soltis, J., Stutz, J., Sweeney, C., Thompson, C. R., Trainer, M. K., Tsai, C., Veres, P. R., Washenfelder, R. A., Warneke, C., Wild, R. J., Young, C. J., Yuan, B., and Zamora, R.: High winter ozone pollution from carbonyl photolysis in an oil and gas basin, Nature, 514, 351–354, https://doi.org/10.1038/nature13767, 2014.

Endresen, Ø.: Emission from international sea transportation and environmental impact, J. Geophys. Res., 108, 29239, https://doi.org/10.1029/2002JD002898, 2003.

Eyring, V.: Emissions from international shipping: 1. The last 50 years, J. Geophys. Res., 110, D17305, https://doi.org/10.1029/2004JD005619, 2005.

Eyring, V., Stevenson, D. S., Lauer, A., Dentener, F. J., Butler, T., Collins, W. J., Ellingsen, K., Gauss, M., Hauglustaine, D. A., Isaksen, I. S. A., Lawrence, M. G., Richter, A., Rodriguez, J. M., Sanderson, M., Strahan, S. E., Sudo, K., Szopa, S., van Noije, T. P. C., and Wild, O.: Multi-model simulations of the impact of international shipping on Atmospheric Chemistry and Climate in 2000 and 2030, Atmos. Chem. Phys., 7, 757–780, https://doi.org/10.5194/acp-7-757-2007, 2007.

Ezhova, E., Ylivinkka, I., Kuusk, J., Komsaare, K., Vana, M., Krasnova, A., Noe, S., Arshinov, M., Belan, B., Park, S.-B., Lavrič, J. V., Heimann, M., Petäjä, T., Vesala, T., Mammarella, I., Kolari, P., Bäck, J., Rannik, Ü., Kerminen, V.-M., and Kulmala, M.: Direct effect of aerosols on solar radiation and gross primary production in boreal and hemiboreal forests, Atmos. Chem. Phys., 18, 17863–17881, https://doi.org/10.5194/acp-18-17863-2018, 2018.

Farahat, A.: Air pollution in the Arabian Peninsula (Saudi Arabia, the United Arab Emirates, Kuwait, Qatar, Bahrain, and Oman): Causes, effects, and aerosol categorization, Arab. J. Geosci., 9, 196, https://doi.org/10.1007/s12517-015-2203-y, 2016.

Fountoukis, C., Ayoub, M. A., Ackermann, L., Perez-Astudillo, D., Bachour, D., Gladich, I., and Hoehn, R. D.: Vertical Ozone Concentration Profiles in the Arabian Gulf Region during Summer and Winter: Sensitivity of WRF-Chem to Planetary Boundary Layer Schemes, Aerosol Air Qual. Res., 18, 1183–1197, https://doi.org/10.4209/aaqr.2017.06.0194, 2018.

Fuchs, H., Novelli, A., Rolletter, M., Hofzumahaus, A., Pfannerstill, E. Y., Kessel, S., Edtbauer, A., Williams, J., Michoud, V., Dusanter, S., Locoge, N., Zannoni, N., Gros, V., Truong, F., Sarda-Esteve, R., Cryer, D. R., Brumby, C. A., Whalley, L. K., Stone, D., Seakins, P. W., Heard, D. E., Schoemaecker, C., Blocquet, M., Coudert, S., Batut, S., Fittschen, C., Thames, A. B., Brune, W. H., Ernest, C., Harder, H., Muller, J. B. A., Elste, T., Kubistin, D., Andres, S., Bohn, B., Hohaus, T., Holland, F., Li, X., Rohrer, F., Kiendler-Scharr, A., Tillmann, R., Wegener, R., Yu, Z., Zou, Q., and Wahner, A.: Comparison of OH reactivity measurements in the atmospheric simulation chamber SAPHIR, Atmos. Meas. Tech., 10, 4023–4053, https://doi.org/10.5194/amt-10-4023-2017, 2017.

Gilman, J. B., Kuster, W. C., Goldan, P. D., Herndon, S. C., Zahniser, M. S., Tucker, S. C., Brewer, W. A., Lerner, B. M., Williams, E. J., Harley, R. A., Fehsenfeld, F. C., Warneke, C., and Gouw, J. A. de: Measurements of volatile organic compounds during the 2006 TexAQS/GoMACCS campaign: Industrial influences, regional characteristics, and diurnal dependencies of the OH reactivity, J. Geophys. Res., 114, D00F06, https://doi.org/10.1029/2008JD011525, 2009.

Gilman, J. B., Lerner, B. M., Kuster, W. C., and de Gouw, J. A.: Source signature of volatile organic compounds from oil and natural gas operations in northeastern Colorado, Environ. Sci. Technol., 47, 1297–1305, https://doi.org/10.1021/es304119a, 2013.

Global Energy Observatory: Abu Sultan Thermal Power Plant Egypt, available at: http://globalenergyobservatory.org/geoid/1977 (last access: 2 January 2019), 2015.

Goldstein, A. H. and Galbally, I. E.: Known and Unexplored Organic Constituents in the Earth's Atmosphere, Environ. Sci. Technol., 41, 1514–1521, https://doi.org/10.1021/es072476p, 2007.

Grosjean, D. and Seinfeld, J. H.: Parameterization of the formation potential of secondary organic aerosols, Atmos. Environ., 23, 1733–1747, https://doi.org/10.1016/0004-6981(89)90058-9, 1989.

Grosjean, E., Williams, E. L., and Grosjean, D.: Atmospheric chemistry of acrolein, Sci. Total Environ., 153, 195–202, https://doi.org/10.1016/0048-9697(94)90198-8, 1994.

Gueneron, M., Erickson, M. H., VanderSchelden, G. S., and Jobson, B. T.: PTR-MS fragmentation patterns of gasoline hydrocarbons, Int. J. Mass Spectrom., 379, 97–109, https://doi.org/10.1016/j.ijms.2015.01.001, 2015.

Haagen-Smit, A. J.: Chemistry and Physiology of Los Angeles Smog, Ind. Eng. Chem., 44, 1342–1346, https://doi.org/10.1021/ie50510a045, 1952.

Hansen, R. F., Blocquet, M., Schoemaecker, C., Léonardis, T., Locoge, N., Fittschen, C., Hanoune, B., Stevens, P. S., Sinha, V., and Dusanter, S.: Intercomparison of the comparative reactivity method (CRM) and pump–probe technique for measuring total OH reactivity in an urban environment, Atmos. Meas. Tech., 8, 4243–4264, https://doi.org/10.5194/amt-8-4243-2015, 2015.

Holz, F., Richter, P. M., and Egging, R.: A Global Perspective on the Future of Natural Gas: Resources, Trade, and Climate Constraints, Rev. Env. Econ. Policy, 9, 85–106, https://doi.org/10.1093/reep/reu016, 2015.

Huang, C., Hu, Q., Wang, H., Qiao, L., Jing, S.'a., Wang, H., Zhou, M., Zhu, S., Ma, Y., Lou, S., Li, L., Tao, S., Li, Y., and Lou, D.: Emission factors of particulate and gaseous compounds from a large cargo vessel operated under real-world conditions, Environ. Pollut., 242, 667–674, https://doi.org/10.1016/j.envpol.2018.07.036, 2018.

IMO: Prevention of Air Pollution from Ships: Revised MARPOL Annex VI, available at: http://www.imo.org/en/OurWork/Environment/PollutionPrevention/AirPollution/Pages/Air-Pollution.aspx, last access: 1 March 2019.

Ingham, T., Goddard, A., Whalley, L. K., Furneaux, K. L., Edwards, P. M., Seal, C. P., Self, D. E., Johnson, G. P., Read, K. A., Lee, J. D., and Heard, D. E.: A flow-tube based laser-induced fluorescence instrument to measure OH reactivity in the troposphere, Atmos. Meas. Tech., 2, 465–477, https://doi.org/10.5194/amt-2-465-2009, 2009.

Johansson, L., Jalkanen, J.-P., and Kukkonen, J.: Global assessment of shipping emissions in 2015 on a high spatial and temporal resolution, Atmos. Environ., 167, 403–415, https://doi.org/10.1016/j.atmosenv.2017.08.042, 2017.

Keßel, S. U.: Entwicklung und Charakterisierung der Comparative Reactivity Method zur Messung von Hydroxylradikal- und Chlorradikal-Reaktivitäten – Troposphärische Oxidationschemie in drei unterschiedlich stark anthropogen beeinflussten Gebieten, Dissertation, Johannes-Gutenberg-Universität, Mainz, 2016.

Khalil, M. A. K., Butenhoff, C. L., Porter, W. C., Almazroui, M., Alkhalaf, A., and Al-Sahafi, M. S.: Air quality in Yanbu, Saudi Arabia, J. Air Waste Manage., 66, 341–355, https://doi.org/10.1080/10962247.2015.1129999, 2016.

Khatib, H.: Oil and natural gas prospects: Middle East and North Africa, Energ. Policy, 64, 71–77, https://doi.org/10.1016/j.enpol.2013.07.091, 2014.

Kim, S., Sanchez, D., Wang, M., Seco, R., Jeong, D., Hughes, S., Barletta, B., Blake, D. R., Jung, J., Kim, D., Lee, G., Lee, M., Ahn, J., Lee, S.-D., Cho, G., Sung, M.-Y., Lee, Y.-H., Kim, D. B., Kim, Y., Woo, J.-H., Jo, D., Park, R., Park, J.-H., Hong, Y.-D., and Hong, J.-H.: OH reactivity in urban and suburban regions in Seoul, South Korea – an East Asian megacity in a rapid transition, Faraday Discuss., 189, 231–251, https://doi.org/10.1039/c5fd00230c, 2016.

Kirchner, F., Jeanneret, F., Clappier, A., Krüger, B., van den Bergh, H., and Calpini, B.: Total VOC reactivity in the planetary boundary layer: 2. A new indicator for determining the sensitivity of the ozone production to VOC and NOx, J. Geophys. Res., 106, 3095–3110, https://doi.org/10.1029/2000JD900603, 2001.

Koppmann, R.: Volatile Organic Compounds in the Atmosphere, Blackwell Publishing Ltd, Oxford, UK, 2007.

Kovacs, T. A., Brune, W. H., Harder, H., Martinez, M., Simpas, J. B., Frost, G. J., Williams, E., Jobson, T., Stroud, C., Young, V., Fried, A., and Wert, B.: Direct measurements of urban OH reactivity during Nashville SOS in summer 1999, J. Environ. Monitor., 5, 68–74, https://doi.org/10.1039/b204339d, 2003.

Kroll, J. H. and Seinfeld, J. H.: Chemistry of secondary organic aerosol: Formation and evolution of low-volatility organics in the atmosphere, Atmos. Environ., 42, 3593–3624, https://doi.org/10.1016/j.atmosenv.2008.01.003, 2008.

Krotkov, N. A., McLinden, C. A., Li, C., Lamsal, L. N., Celarier, E. A., Marchenko, S. V., Swartz, W. H., Bucsela, E. J., Joiner, J., Duncan, B. N., Boersma, K. F., Veefkind, J. P., Levelt, P. F., Fioletov, V. E., Dickerson, R. R., He, H., Lu, Z., and Streets, D. G.: Aura OMI observations of regional SO_2 and NO_2 pollution changes from 2005 to 2015, Atmos. Chem. Phys., 16, 4605–4629, https://doi.org/10.5194/acp-16-4605-2016, 2016.

Lelieveld, J., Hoor, P., Jöckel, P., Pozzer, A., Hadjinicolaou, P., Cammas, J.-P., and Beirle, S.: Severe ozone air pollution in the Persian Gulf region, Atmos. Chem. Phys., 9, 1393–1406, https://doi.org/10.5194/acp-9-1393-2009, 2009.

Lelieveld, J., Hadjinicolaou, P., Kostopoulou, E., Chenoweth, J., El Maayar, M., Giannakopoulos, C., Hannides, C., Lange, M. A., Tanarhte, M., Tyrlis, E., and Xoplaki, E.: Climate change and impacts in the Eastern Mediterranean and the Middle East, Climatic Change, 114, 667–687, https://doi.org/10.1007/s10584-012-0418-4, 2012.

Lelieveld, J., Evans, J. S., Fnais, M., Giannadaki, D., and Pozzer, A.: The contribution of outdoor air pollution sources to premature mortality on a global scale, Nature, 525, 367–371, https://doi.org/10.1038/nature15371, 2015.

Lelieveld, J., Proestos, Y., Hadjinicolaou, P., Tanarhte, M., Tyrlis, E., and Zittis, G.: Strongly increasing heat extremes in the Middle East and North Africa (MENA) in the 21st century, Climatic Change, 137, 245–260, https://doi.org/10.1007/s10584-016-1665-6, 2016.

Lindinger, W. and Jordan, A.: Proton-transfer-reaction mass spectrometry (PTR–MS): On-line monitoring of volatile organic compounds at pptv levels, Chem. Soc. Rev., 27, 347–354, https://doi.org/10.1039/a827347z, 1998.

Mao, J., Ren, X., Chen, S., Brune, W. H., Chen, Z., Martinez, M., Harder, H., Lefer, B., Rappenglück, B., Flynn, J., and Leuchner, M.: Atmospheric oxidation capacity in the summer of Houston 2006: Comparison with summer measurements in other metropolitan studies, Atmos. Environ., 44, 4107–4115, https://doi.org/10.1016/j.atmosenv.2009.01.013, 2010.

Matysik, S., Ramadan, A. B., and Schlink, U.: Spatial and temporal variation of outdoor and indoor exposure of volatile organic compounds in Greater Cairo, Atmos. Pollut. Res., 1, 94–101, https://doi.org/10.5094/APR.2010.012, 2010.

Mertens, M., Grewe, V., Rieger, V. S., and Jöckel, P.: Revisiting the contribution of land transport and shipping emissions to tropospheric ozone, Atmos. Chem. Phys., 18, 5567–5588, https://doi.org/10.5194/acp-18-5567-2018, 2018.

Michoud, V., Hansen, R. F., Locoge, N., Stevens, P. S., and Dusanter, S.: Detailed characterizations of the new Mines Douai comparative reactivity method instrument via laboratory experiments and modeling, Atmos. Meas. Tech., 8, 3537–3553, https://doi.org/10.5194/amt-8-3537-2015, 2015.

Milazzo, M. F., Ancione, G., and Lisi, R.: Emissions of volatile organic compounds during the ship-loading of petroleum products: Dispersion modelling and environmental concerns, J. Environ. Manage., 204, 637–650, https://doi.org/10.1016/j.jenvman.2017.09.045, 2017.

Moradzadeh, M., Ashrafi, k., and Shafiepour-Motlagh, M.: The Evaluation of Tropospheric Ozone Formation in the Downwind of the South Pars Industrial Zone, Pollution, 5, 361–375, https://doi.org/10.22059/poll.2018.269218.539, 2019.

Nakashima, Y., Kato, S., Greenberg, J., Harley, P., Karl, T., Turnipseed, A., Apel, E., Guenther, A., Smith, J., and Kajii, Y.: Total OH reactivity measurements in ambient air in a southern Rocky mountain ponderosa pine forest during BEACHON-SRM08 summer campaign, Atmos. Environ., 85, 1–8, https://doi.org/10.1016/j.atmosenv.2013.11.042, 2014.

Overland, I.: Future Petroleum Geopolitics: Consequences of Climate Policy and Unconventional Oil and Gas, in: Handbook of Clean Energy Systems, edited by: Yan, J., Wiley, Weinheim, 1–29, 2015.

Parrish, D. D., Trainer, M., Holloway, J. S., Yee, J. E., Warshawsky, M. S., Fehsenfeld, F. C., Forbes, G. L., and Moody, J. L.: Relationships between ozone and carbon monoxide at surface sites in the North Atlantic region, J. Geophys. Res., 103, 13357–13376, https://doi.org/10.1029/98JD00376, 1998.

Pfannerstill, E. Y., Nölscher, A. C., Yáñez-Serrano, A. M., Bourtsoukidis, E., Keßel, S., Janssen, R. H. H., Tsokankunku, A., Wolff, S., Sörgel, M., Sá, M. O., Araújo, A., Walter, D., Lavrič, J., Dias-Júnior, C. Q., Kesselmeier, J., and Williams, J.: Total OH Reactivity Changes Over the Amazon Rainforest During an El Niño Event, Front. For. Glob. Change, 1, 600, https://doi.org/10.3389/ffgc.2018.00012, 2018.

Pfannerstill, E. Y., Wang, N., and Williams, J.: Total OH reactivity measured around the Arabian Peninsula July–August 2017, https://doi.org/10.5281/zenodo.3354117, 2019.

Praplan, A. P., Pfannerstill, E. Y., Williams, J., and Hellén, H.: OH reactivity of the urban air in Helsinki, Finland, during winter, Atmos. Environ., 169, 150–161, https://doi.org/10.1016/j.atmosenv.2017.09.013, 2017.

Pusede, S. E. and Cohen, R. C.: On the observed response of ozone to NO_X and VOC reactivity reductions in San Joaquin Valley California 1995–present, Atmos. Chem. Phys., 12, 8323–8339, https://doi.org/10.5194/acp-12-8323-2012, 2012.

Pusede, S. E., Gentner, D. R., Wooldridge, P. J., Browne, E. C., Rollins, A. W., Min, K.-E., Russell, A. R., Thomas, J., Zhang, L., Brune, W. H., Henry, S. B., DiGangi, J. P., Keutsch, F. N., Harrold, S. A., Thornton, J. A., Beaver, M. R., St. Clair, J. M., Wennberg, P. O., Sanders, J., Ren, X., VandenBoer, T. C., Markovic, M. Z., Guha, A., Weber, R., Goldstein, A. H., and Cohen, R. C.: On the temperature dependence of organic reactivity, nitrogen oxides, ozone production, and the impact

of emission controls in San Joaquin Valley, California, Atmos. Chem. Phys., 14, 3373–3395, https://doi.org/10.5194/acp-14-3373-2014, 2014.

Ren, X., Brune, W. H., Cantrell, C. A., Edwards, G. D., Shirley, T., Metcalf, A. R., and Lesher, R. L.: Hydroxyl and Peroxy Radical Chemistry in a Rural Area of Central Pennsylvania: Observations and Model Comparisons, J. Atmos. Chem., 52, 231–257, https://doi.org/10.1007/s10874-005-3651-7, 2005.

Ren, X., Brune, W. H., Oliger, A., Metcalf, A. R., Simpas, J. B., Shirley, T., Schwab, J. J., Bai, C., Roychowdhury, U., Li, Y., Cai, C., Demerjian, K. L., He, Y., Zhou, X., Gao, H., and Hou, J.: OH, HO_2 and OH reactivity during the PMTACS-NY Whiteface Mountain 2002 campaign: Observations and model comparison, J. Geophys. Res., 111, D10S03, https://doi.org/10.1029/2005JD006126, 2006.

Ren, X., van Duin, D., Cazorla, M., Chen, S., Mao, J., Zhang, L., Brune, W. H., Flynn, J. H., Grossberg, N., Lefer, B. L., Rappenglück, B., Wong, K. W., Tsai, C., Stutz, J., Dibb, J. E., Thomas Jobson, B., Luke, W. T., and Kelley, P.: Atmospheric oxidation chemistry and ozone production: Results from SHARP 2009 in Houston, Texas, J. Geophys. Res.-Atmos., 118, 5770–5780, https://doi.org/10.1002/jgrd.50342, 2013.

Salameh, T., Afif, C., Sauvage, S., Borbon, A., and Locoge, N.: Speciation of non-methane hydrocarbons (NMHCs) from anthropogenic sources in Beirut, Lebanon, Environ. Sci. Pollut. Res., 21, 10867–10877, https://doi.org/10.1007/s11356-014-2978-5, 2014.

Salameh, T., Sauvage, S., Afif, C., Borbon, A., and Locoge, N.: Source apportionment vs. emission inventories of non-methane hydrocarbons (NMHC) in an urban area of the Middle East: local and global perspectives, Atmos. Chem. Phys., 16, 3595–3607, https://doi.org/10.5194/acp-16-3595-2016, 2016.

Schade, G. W. and Roest, G.: Analysis of non-methane hydrocarbon data from a monitoring station affected by oil and gas development in the Eagle Ford shale, Texas, Elem. Sci. Anth., 4, 000096, https://doi.org/10.12952/journal.elementa.000096, 2016.

Schauer, J. J., Kleeman, M. J., Cass, G. R., and Simoneit, B. R. T.: Measurement of Emissions from Air Pollution Sources. 5. $C1 - C32$ Organic Compounds from Gasoline-Powered Motor Vehicles, Environ. Sci. Technol., 36, 1169–1180, https://doi.org/10.1021/es0108077, 2002.

Sillman, S.: The relation between ozone, NOx and hydrocarbons in urban and polluted rural environments, Atmos. Environ., 33, 1821–1845, https://doi.org/10.1016/S1352-2310(98)00345-8, 1999.

Simpson, I. J., Aburizaiza, O. S., Siddique, A., Barletta, B., Blake, N. J., Gartner, A., Khwaja, H., Meinardi, S., Zeb, J., and Blake, D. R.: Air quality in Mecca and surrounding holy places in Saudi Arabia during Hajj: Initial survey, Environ. Sci. Technol., 48, 8529–8537, https://doi.org/10.1021/es5017476, 2014.

Sinha, V., Williams, J., Crowley, J. N., and Lelieveld, J.: The Comparative Reactivity Method – a new tool to measure total OH Reactivity in ambient air, Atmos. Chem. Phys., 8, 2213–2227, https://doi.org/10.5194/acp-8-2213-2008, 2008.

Sinha, V., Williams, J., Lelieveld, J., Ruuskanen, T. M., Kajos, M. K., Patokoski, J., Hellen, H., Hakola, H., Mogensen, D., Boy, M., Rinne, J., and Kulmala, M.: OH reactivity measurements within a boreal forest: evidence for unknown

reactive emissions, Environ. Sci. Technol., 44, 6614–6620, https://doi.org/10.1021/es101780b, 2010.

Sinha, V., Williams, J., Diesch, J. M., Drewnick, F., Martinez, M., Harder, H., Regelin, E., Kubistin, D., Bozem, H., Hosaynali-Beygi, Z., Fischer, H., Andrés-Hernández, M. D., Kartal, D., Adame, J. A., and Lelieveld, J.: Constraints on instantaneous ozone production rates and regimes during DOMINO derived using in-situ OH reactivity measurements, Atmos. Chem. Phys., 12, 7269–7283, https://doi.org/10.5194/acp-12-7269-2012, 2012.

Smoydzin, L., Fnais, M., and Lelieveld, J.: Ozone pollution over the Arabian Gulf – role of meteorological conditions, Atmos. Chem. Phys. Discuss., 12, 6331–6361, https://doi.org/10.5194/acpd-12-6331-2012, 2012.

Sudo, K. and Akimoto, H.: Global source attribution of tropospheric ozone: Long-range transport from various source regions, J. Geophys. Res., 112, 1609, https://doi.org/10.1029/2006JD007992, 2007.

Suez Canal Authority: Navigation Statistics, available at: https://www.suezcanal.gov.eg/English/Navigation/Pages/NavigationStatistics.aspx (last access: 1 February 2019b), 2017.

Suez Canal Authority: Canal Characteristics, available at: https://www.suezcanal.gov.eg/English/About/SuezCanal/Pages/CanalCharacteristics.aspx (last access: 1 February 2019a), 2018.

Swarthout, R. F., Russo, R. S., Zhou, Y., Hart, A. H., and Sive, B. C.: Volatile organic compound distributions during the NACHTT campaign at the Boulder Atmospheric Observatory: Influence of urban and natural gas sources, J. Geophys. Res.-Atmos., 118, 10614–10637, https://doi.org/10.1002/jgrd.50722, 2013.

Tanarhte, M., Hadjinicolaou, P., and Lelieveld, J.: Intercomparison of temperature and precipitation data sets based on observations in the Mediterranean and the Middle East, J. Geophys. Res., 117, D12102, https://doi.org/10.1029/2011JD017293, 2012.

Terink, W., Immerzeel, W. W., and Droogers, P.: Climate change projections of precipitation and reference evapotranspiration for the Middle East and Northern Africa until 2050, Int. J. Climatol., 33, 3055–3072, https://doi.org/10.1002/joc.3650, 2013.

Warneke, C. and de Gouw, J. A.: Organic trace gas composition of the marine boundary layer over the northwest Indian Ocean in April 2000, Atmos. Environ., 35, 5923–5933, https://doi.org/10.1016/S1352-2310(01)00384-3, 2001.

Wasimi, S. A.: Climate change in the Middle East and North Africa (MENA) region and implications for water resources project planning and management, Int. J. Cl. Chan. Strat. Man., 2, 297–320, https://doi.org/10.1108/17568691011063060, 2010.

Wei, W., Cheng, S., Li, G., Wang, G., and Wang, H.: Characteristics of ozone and ozone precursors (VOCs and NOx) around a petroleum refinery in Beijing, China, J.Environ. Sci., 26, 332–342, https://doi.org/10.1016/S1001-0742(13)60412-X, 2014.

Williams, J. and Brune, W.: A roadmap for OH reactivity research, Atmos. Environ., 106, 371–372, https://doi.org/10.1016/j.atmosenv.2015.02.017, 2015.

Williams, J., Keßel, S. U., Nölscher, A. C., Yang, Y., Lee, Y., Yáñez-Serrano, A. M., Wolff, S., Kesselmeier, J., Klüpfel, T., Lelieveld, J., and Shao, M.: Opposite OH reactivity and ozone cycles in the Amazon rainforest and megacity Beijing: Subversion of biospheric oxidant control by anthropogenic emissions, Atmos. Environ., 125, 112–118, https://doi.org/10.1016/j.atmosenv.2015.11.007, 2016.

Wu, Y., Yang, Y.-D., Shao, M., and Lu, S.-H.: Missing in total OH reactivity of VOCs from gasoline evaporation, Chinese Chem. Lett., 26, 1246–1248, https://doi.org/10.1016/j.cclet.2015.05.047, 2015.

Xiao, Q., Li, M., Liu, H., Fu, M., Deng, F., Lv, Z., Man, H., Jin, X., Liu, S., and He, K.: Characteristics of marine shipping emissions at berth: profiles for particulate matter and volatile organic compounds, Atmos. Chem. Phys., 18, 9527–9545, https://doi.org/10.5194/acp-18-9527-2018, 2018.

Yang, Y., Shao, M., Wang, X., Nölscher, A. C., Kessel, S., Guenther, A., and Williams, J.: Towards a quantitative understanding of total OH reactivity: A review, Atmos. Environ., 134, 147–161, https://doi.org/10.1016/j.atmosenv.2016.03.010, 2016.

Yang, Y., Shao, M., Keßel, S., Li, Y., Lu, K., Lu, S., Williams, J., Zhang, Y., Zeng, L., Nölscher, A. C., Wu, Y., Wang, X., and Zheng, J.: How the OH reactivity affects the ozone production efficiency: case studies in Beijing and Heshan, China, Atmos. Chem. Phys., 17, 7127–7142, https://doi.org/10.5194/acp-17-7127-2017, 2017.

Yoshino, A., Sadanaga, Y., Watanabe, K., Kato, S., Miyakawa, Y., Matsumoto, J., and Kajii, Y.: Measurement of total OH reactivity by laser-induced pump and probe technique–comprehensive observations in the urban atmosphere of Tokyo, Atmos. Environ., 40, 7869–7881, https://doi.org/10.1016/j.atmosenv.2006.07.023, 2006.

Zhang, X., Aguilar, E., Sensoy, S., Melkonyan, H., Tagiyeva, U., Ahmed, N., Kutaladze, N., Rahimzadeh, F., Taghipour, A., Hantosh, T. H., Albert, P., Semawi, M., Karam Ali, M., Said Al-Shabibi, M. H., Al-Oulan, Z., Zatari, T., Al Dean Khelet, I., Hamoud, S., Sagir, R., Demircan, M., Eken, M., Adiguzel, M., Alexander, L., Peterson, T. C., and Wallis, T.: Trends in Middle East climate extreme indices from 1950 to 2003, J. Geophys. Res., 110, 1959, https://doi.org/10.1029/2005JD006181, 2005.

Zhang, Y., Cooper, O. R., Gaudel, A., Thompson, A. M., Nédélec, P., Ogino, S.-Y., and West, J. J.: Tropospheric ozone change from 1980 to 2010 dominated by equatorward redistribution of emissions, Natu. Geosci., 9, 875–879, https://doi.org/10.1038/ngeo2827, 2016.

Zhao, Y., Saunois, M., Bousquet, P., Lin, X., Hegglin, M. I., Canadell, J. G., Jackson, R. B., Hauglustaine, D. A., Szopa, S., Stavert, A. R., Abraham, N. L., Archibald, A. T., Bekki, S., Deushi, M., Jöckel, P., Josse, B., Kinnison, D., Kirner, O., Marécal, V., O'Connor, F. M., Plummer, D. A., Revell, L. E., Rozanov, E., Stenke, A., Strode, S., Tilmes, S., Dlugokencky, E. J., and Zheng, B.: Inter-model comparison of global hydroxyl radical (OH) distributions and their impact on atmospheric methane over the 2000–2016 period, Atmos. Chem. Phys. Discuss., https://doi.org/10.5194/acp-2019-281, in review, 2019.